Title: Anthranilic acid regulates subcellular localization of auxin transporters during root gravitropism

Authors: Siamsa M. Doyle[1]*, Adeline Rigal[1]*, Peter Grones[1#], Michal Karady[1#], Deepak K. Barange[1,2], Mateusz Majda[1], Barbora Pařízková[3], Michael Karampelias[4], Marta Zwiewka[5], Aleš Pěnčik[1], Fredrik Almqvist[2], Karin Ljung[1], Ondřej Novák[1,3] and Stéphanie Robert[1]

[1]Umeå Plant Science Centre (UPSC), Department of Forest Genetics and Plant Physiology, Swedish University of Agricultural Sciences (SLU), Umeå, Sweden.
[2]Department of Chemistry, Umeå University, Umeå, Sweden.
[3]Laboratory of Growth Regulators, Centre of the Region Haná for Biotechnological and Agricultural Research, Faculty of Science of Palacký University & Institute of Experimental Botany CAS, Šlechtitelů 27, Olomouc, Czech Republic.
[4]Department of Plant Systems Biology, Vlaams Instituut voor Biotechnologie (VIB), and Department of Plant Biotechnology and Bioinformatics, Ghent University, Gent, Belgium.
[5]Central European Institute of Technology (CEITEC), Masaryk University, Brno, Czech Republic.
*These authors contributed equally to this work.
[#]These authors contributed equally to this work.

Present affiliations: D. K. Barange's present afiliation is Department of Chemistry, Colorado State University, Fort Collins, Colorado, USA. M. Majda's present affiliation is Department of Comparative Development and Genetics, Max Planck Institute for Plant Breeding Research, Köln, Germany. M. Karampelias's present affiliation is Centre for Research in Agricultural Genomics (CRAG) CSIC-IRTA-UAB-UB, Barcelona, Spain.

Corresponding author: Stéphanie Robert (stephanie.robert@slu.se)

Abstract

The distribution of the phytohormone auxin within plant tissues is of great importance for developmental plasticity, including root gravitropic growth. Auxin flow is directed by the subcellular polar distribution and dynamic relocalization of plasma membrane-localized auxin transporters such as the PIN-FORMED (PIN) efflux carriers, which are in turn regulated by complex endomembrane trafficking pathways. Anthranilic acid (AA) is an important early precursor of the main natural plant auxin indole-3-acetic acid (IAA). We took advantage of an AA-deficient, and consequently IAA-deficient, mutant displaying agravitropic root growth to show that AA rescues root gravitropic growth at

concentrations that do not rescue IAA levels. Treatments with, or deficiency in, AA result in defects in PIN polarity and gravistimulus-induced PIN relocalization within root cells. Taken together, our results reveal a previously unknown role for AA in the regulation of PIN subcellular localization and dynamics involved in root gravitropism, which is independent of its better-known role in IAA biosynthesis.

Introduction

The distribution of the phytohormone auxin in controlled concentration gradients within certain tissues and organs plays an important role in regulating the dynamically plastic growth and development of plants (Vanneste and Friml, 2009). Over the past couple of decades, an intense research effort has revealed many of the complex mechanisms by which plasma membrane-localized auxin carrier proteins are polarly distributed in order to direct the flow of auxin in plant tissues and maintain these gradients (reviewed by Luschnig and Vert, 2014; and Naramoto, 2017). These proteins, including the well-studied PIN-FORMED (PIN) auxin efflux carriers, are remarkably dynamic in that they rapidly relocalize within the cell in response to signals, becoming more or less polar or shifting the direction of their polarity entirely. This dynamic responsiveness, which is facilitated by vesicular cycling and complex endomembrane trafficking pathways, is essential for altering the direction and strength of cell-to-cell auxin flow and redistributing auxin in response to external cues, thereby regulating cell and tissue growth and plasticity.

Root development in *Arabidopsis thaliana* has received particular attention as a model system demonstrating the importance of auxin gradients for plant growth and development (Clark et al., 2014). Mutations affecting auxin transporters often disturb root gravitropism and specific PIN proteins within the root tip have been shown to relocalize in response to changes in the gravity vector, leading to changes in auxin flow and consequently, organ growth adjustment (reviewed by Geisler et al., 2014). PIN2 in the root tip epidermis is particularly important for this response; being apically (shootward) polarized within epidermal cells (Müller et al., 1998), PIN2 transports auxin upwards in this tissue, contributing in a concerted manner together with other PIN proteins to the maintenance of the auxin maximum required in the root apical meristem for proper root development (Adamowski and Friml, 2015). However, in the case of a

reorientation of the root to a horizontal position, PIN2 is rapidly redistributed from the plasma membrane to the vacuole within epidermal cells at the upper organ side (Kleine-Vehn et al., 2008; Abas et al., 2006). This results in accumulation of auxin and consequent inhibition of cell elongation at the lower root side, leading to the root tip bending downwards towards the gravity vector. In the root columella, the cellular relocalization of PIN3 and PIN7 has also been shown to play an important role in root gravitropic growth responses. While these PIN proteins are generally apolar in columella cells, they redistribute towards the basal (rootward) plasma membranes upon reorientation of the root (Friml et al., 2002b; Kleine-Vehn et al., 2010), which is presumed to redirect the flow of auxin within the columella, thus further contributing to auxin accumulation at the lower root side.

Despite our knowledge on the mechanisms of PIN polarity and redistribution, a lot of information is still lacking regarding the regulation of PIN dynamics. In our previous work, we employed a chemical biology approach, whereby we isolated and characterized small synthetic molecules selectively altering the polarity of specific PIN proteins, to dissect the trafficking pathways involved in regulating their localization (Doyle et al., 2015a). This approach led us to identify a potential role for the endogenous compound anthranilic acid (AA) in PIN polarity regulation, which we investigate in the current study. AA is an important early precursor of the main natural plant auxin indole-3-acetic acid (IAA) (Maeda and Dudareva, 2012) and as auxin itself has been shown to regulate PIN polarity in a feedback mechanism to control its own flow (Paciorek et al., 2005), we hypothesized that AA may play a similar regulatory role. Herein, using *Arabidopsis* root gravitropism as a model system for auxin-regulated plastic growth, we provide strong evidence in favor of this hypothesis. Ultimately, we reveal a previously unknown role for the IAA precursor AA in the regulation of PIN polarity and relocalization required for root gravitropic responses and furthermore, we show that this role of AA is distinct from its well-known role in IAA biosynthesis.

Results

AA rescues root gravitropic growth and length differently in an AA-deficient mutant

Using a chemical biology approach, we previously isolated the small synthetic molecule Endosidin 8 (ES8), which disturbs the polarity of selective PIN proteins in the root of

Arabidopsis thaliana, leading to an altered root auxin distribution pattern and defective root growth (Doyle et al., 2015a). Intriguingly, the chemical structure of ES8 reveals that this molecule is an analog of the endogenous plant compound AA (Fig. 1 A), a precursor of tryptophan (Trp), the main precursor of the predominant plant auxin IAA (Ljung, 2013; Zhao, 2014). This prompted us to question whether endogenous AA might play a role in growth and development of the root. We therefore investigated the root phenotype of a loss-of-function *Arabidopsis* mutant in both the *ANTHRANILATE SYNTHASE SUBUNIT ALPHA1* gene (*ASA1*, also known as the *WEAK ETHYLENE INSENSITIVE2* gene, *WEI2*) and the *ANTHRANILATE SYNTHASE SUBUNIT BETA1* gene (*ASB1*, also known as *WEI7*). In the double mutant, *wei2wei7* (Ikeda et al., 2009; Stepanova et al., 2005), the AA level is presumed to be reduced, which is supported by the rescue of an ethylene sensitivity phenotype in the single *wei2-1* and *wei7-1* mutants by treatment with AA (Stepanova et al., 2005). To confirm this, we analyzed the levels of several IAA precursors/catabolites in the mutant and the wild type (WT) Columbia-0 (Col-0), revealing that AA content was indeed significantly reduced in *wei2wei7* compared to Col-0, as were the levels of the IAA precursors Trp, indole-3-acetonitrile (IAN) and indole-3-acetimide (IAM) (Fig. S1), most likely due to the decreased AA content. However, neither the IAA precursor tryptamine (Tra) nor catabolite 2-oxoindole-3-acetic acid (oxIAA) showed altered content in the mutant compared to the WT (Fig. S1).

We were interested in the strong agravitropic and short phenotypes of *wei2wei7* roots compared to WT Col-0 seedlings (Fig. 1 B and C), considering that ES8 treatment reduces both gravitropic root growth and root length in Col-0 (Doyle et al., 2015a). To investigate AA-mediated rescue of these root phenotypes in *wei2wei7*, we performed long-term AA treatments by growing WT and mutant seedlings on medium supplemented with a range of AA concentrations. In Col-0, none of the tested concentrations affected gravitropic root growth, while concentrations of 10 µM or more decreased root length in a dose-dependent manner (Fig. S2 A). As expected, in *wei2wei7* both root gravitropic growth and length were rescued by AA (Fig. 1 C and D), however we observed a striking difference between the AA rescue patterns of these two root phenotypes. While root gravitropic growth in the mutant was fully rescued to WT levels at all AA concentrations applied, root length rescue was concentration-dependent,

with maximal rescue at 5 µM (Fig. 1 D). Furthermore, root length in the mutant was only partially rescued at all AA concentrations applied (Fig. 1 D), compared to WT root length (Fig. S2 A). We hypothesized that the different rescue patterns of root gravitropic growth and length phenotypes by AA in *wei2wei7* might reflect two different roles of AA, one known role in auxin biosynthesis and a distinct, as yet unknown role in regulating auxin distribution, considering that ES8 disturbs auxin distribution patterns in the root (Doyle et al., 2015a).

We next investigated whether ES8, as an analog of AA, could rescue either root gravitropic growth or length in *wei2wei7*. While long-term treatments with increasing concentrations of ES8 decreased both root gravitropic growth and length in a dose-dependent manner in Col-0 (Fig. S2 B), only the highest ES8 concentrations (15 and 20 µM) decreased root gravitropic growth and length in *wei2wei7* (Fig. 1 E). Moreover, while root length was not rescued in the mutant at any ES8 concentration (Fig. 1 E), 5 µM ES8 partially rescued the root gravitropic phenotype of the mutant (Fig. 1 C and E). The partial root gravitropic rescue of *wei2wei7* by ES8 without any effect on root length supported our hypothesis that the gravitropic rescue of *wei2wei7* by AA may be due to a role of AA other than that in auxin biosynthesis.

To further test our hypothesis, we attempted to replicate these results using another analog of both ES8 and AA - ES8 analog no. 7 (ES8.7; Fig. S3 A; ES8 analogs ES8.1 to 6 were previously described by Doyle et al. (2015a)). We also tested the control compound ES8.7-Trp, in which the AA was exchanged for a Trp (Fig. S3 B). In Col-0, long-term ES8.7 treatment at a range of concentrations revealed a similar but weaker effect than ES8 on reduction of root gravitropic growth and length (Fig. S3 C). Strikingly, ES8.7 had a stronger effect than ES8 in rescuing root gravitropic growth in *wei2wei7*, significantly rescuing this phenotype at a range of concentrations from 1 to 15 µM, with almost no effects on root length (Fig. S3 A and D). Moreover, ES8.7-Trp had almost no effect on root gravitropic growth or length at any concentration in both Col-0 (Fig. S3 E) and *wei2wei7* (Fig. S3 B and F). These results strongly suggest that it is the AA part of the ES8 compounds, and not any other part of the molecules, that rescues gravitropic growth of *wei2wei7* roots.

To investigate the possibility that the ES8 compounds might be degraded or metabolized during our experiments to release AA or Trp, we performed both short-

term and long-term treatments of Col-0 and *wei2wei7* seedlings with the ES8 compounds, followed by compound analysis (Fig. S4). We measured the concentrations of the relevant ES8 compound, AA or Trp and the non-AA or non-Trp part of the ES8 compound *in planta* as well as in ES8 compound-supplemented medium to which no seedlings were added. Our results showed that after short-term treatment (5 hours incubation in liquid treatment medium) with 5 µM ES8, high levels of ES8 were detectable in the seedlings and the seedling-free treatment medium remained at about 5 µM ES8 (Fig. S4 A). After long-term treatment (9 days of growth on solid treatment medium), the concentrations of ES8 in the seedlings and the seedling-free treatment medium had lowered considerably, suggesting degradation of ES8 over time. Compared to ES8, much lower levels of ES8.7 and ES8.7-Trp were present in the seedlings after short-term treatment (Fig. S4 B and C), suggesting that ES8 may be more efficiently taken up into seedling tissues or ES8.7 and ES8.7-Trp may be degraded or metabolized during the short-term treatment. Degradation of ES8.7-Trp was supported by our measurements of its concentration in the seedling-free treatment medium, which had already lowered to 3.3 µM after short-term incubation and to 0.5 µM after long-term incubation (Fig. S4 C). Moreover, the levels of ES8.7-Trp in the seedlings were considerably lower after long-term compared to short-trem treatment. While these results suggest that ES8 and ES8.7-Trp are likely degraded over time, the levels of AA and Trp in the seedlings after ES8 compound treatment were not different to the levels after mock treatment and neither AA nor Trp were detected in the treatment medium samples (Fig. S4 D and E). Furthermore, we did not detect non-AA or non-Trp parts of the ES8 compounds at any time point, neither in the seedlings nor in the seedling-free treatment medium (Fig. S4 F). Therefore, the observed activities of the ES8 compounds are not due to the release of AA or Trp and are therefore unlikely to be due to increased IAA biosynthesis.

AA and ES8 can rescue root gravitropic growth in wei2wei7 *without rescuing IAA level*

As AA is a precursor of IAA, an essential regulator of root growth (Goh et al., 2014; Clark et al., 2014), we investigated the possibility that the rescue of root gravitropic growth by ES8 and AA might indirectly result from increased IAA biosynthesis. We

therefore investigated the effects of these compounds on levels of IAA. First, we measured IAA concentrations in Col-0 and *wei2wei7* seedlings after long-term treatments with different concentrations of AA. We found a significant reduction of IAA content in *wei2wei7* compared to Col-0 in control conditions (Fig. 2 A). In Col-0, only treatment with 10 µM AA significantly increased the IAA level (Fig. 2 A). Raised IAA concentrations are therefore the most likely reason why treatments of Col-0 with 10 µM and higher concentrations of AA resulted in significantly shorter roots (Fig. S2 A). While treatment of *wei2wei7* with 1 or 10 µM AA rescued the IAA level to that of mock-treated Col-0, treatment with 0.5 µM AA had no effect on IAA content (Fig. 2 A), despite this concentration having fully rescued root gravitropic growth and partially rescued root length in *wei2wei7* seedlings (Fig. 1 D). Next, we measured IAA content in Col-0 and *wei2wei7* seedlings treated long-term with 5 µM ES8, ES8.7 or ES8.7-Trp. While the IAA level was slightly but significantly reduced in mock-treated *wei2wei7* compared to Col-0, none of the ES8 compounds significantly affected IAA content compared to mock treatment in either genotype (Fig. 2 B). Taken together, these results suggest that AA might play a role in the regulation of root gravitropic growth independently from its function in IAA biosynthesis.

Root gravitropic response is impaired by AA when its conversion to downstream IAA precursors is repressed

To test our hypothesis that AA may regulate root gravitropic growth via a role independent of IAA biosynthesis, we aimed to generate transformed *Arabidopsis* lines in which the gene encoding ASA1 (Niyogi and Fink, 1992) is constitutively overexpressed and that encoding PHOSPHORIBOSYLANTHRANILATE TRANSFERASE 1 (PAT1), which converts AA to the next downstream IAA precursor (Rose et al., 1992), is subject to estradiol-induced silencing. Of several homozygously transformed *35S::ASA1* and *XVE::amiRNA-PAT1* lines, we used qPCR analysis of *ASA1* and *PAT1* expression (Fig. S5 A and B) to select two lines for each construct displaying reproducible and strong constitutive *ASA1* induction (*35S::ASA1* lines 3B6 and 3B7) or inducible *PAT1* silencing (*XVE::amiRNA-PAT1* lines 2D4 and 4B10). We then crossed the selected lines and used qPCR to analyze *ASA1* and *PAT1* expression in the homozygous crosses, which we named *AxP* (*ASA1 x PAT1*) lines (Fig. S5 C and D).

While *ASA1* was overexpressed in all *AxP* lines, there was a tendency for increased *PAT1* expression in non-estradiol-induced conditions in those lines with highest *ASA1* expression, suggesting positive regulation between *ASA1* and *PAT1* genes. We selected two *AxP* lines for further experiments; *AxP1* (3B6x2D4 line no. 4) in which *ASA1* was 5-fold overexpressed compared to the non-treated WT without affecting non-induced *PAT1* expression and *AxP2* (3B7x2D4 line no. 21), in which *ASA1* was 10-fold overexpressed, resulting in 3-fold overexpression of *PAT1* in non-induced conditions (Fig. S5 C and D). Additionally, an estradiol-inducible 5- and 3-fold reduction in *PAT1* expression compared to non-treated Col-0 was shown for *AxP1* and *AxP2*, respectively (Fig. S5 D).

To dissect the effects of *ASA1* overexpression and simultaneous silencing of *PAT1* on the IAA biosynthetic pathway, we analyzed the levels of IAA and several IAA precursors/conjugates/catabolites in WT and *AxP* lines treated long-term with estradiol (grown on supplemented medium). We found that while AA levels tended to be higher in both *AxP* lines than in the WT, the levels of the precursors Trp, IAN and IAM were more variable between the two *AxP* lines (Fig. S6 A). Importantly, the IAA content was not affected in the *AxP* lines compared to the WT, while the conjugates IAA-aspartate (IAAsp) and IAA-glutamate (IAGlu) and the catabolite oxIAA showed reduced levels in the transformed lines compared to the WT (Fig. S6 A). These results suggest that simultaneous overexpression of *ASA1* and silencing of *PAT1* result in increased AA levels, but do not alter IAA levels, perhaps due to a reduced conversion of IAA to IAA conjugates and catabolites.

We next investigated the root phenotypes of the *AxP* lines. In control conditions without estradiol treatment, both lines displayed similar root gravitropic growth to that of the WT (Fig. S6 B), while having slightly shorter roots than the WT (Fig. S6 C). After long-term estradiol treatment, the gravitropic growth of WT and *AxP* roots was slightly reduced, to a similar extent (Fig. S6 B). While long-term estradiol treatment significantly reduced the root length of all genotypes, the treatment affected the *AxP* lines more severely than the WT (Fig. S6 C). To analyze root gravitropic responses in the *AxP* lines, we turned the seedlings 90° and subsequently measured the gravistimulated root bending angles (Fig. S6 D). In control conditions, Col-0 and both *AxP* lines responded to the gravistimulus with a very similar range of root bending

angles, with the majority of roots bending 75-105° (Fig. 3). Estradiol treatment inhibited the gravitropic response of Col-0 roots, reducing their bending angles, resulting in a reduction in the proportion of roots bending 75-105° and an increase in the proportion bending <75° (Fig. 3 A and B). The *AxP* lines, however, responded somewhat differently to estradiol than the WT. As for the WT, estradiol treatment resulted in both a reduction in the proportion of *AxP* roots bending 75-105° and an increase in the proportion bending <75° but additionally resulted in an increase in the proportion bending >105° (Fig. 3 C-F). Therefore, while estradiol treatment specifically reduces root bending in response to a gravitropic stimulus in the WT, the same treatment results in both under- and over-bending of roots in response to a gravistimulus in both *AxP* lines, strongly suggesting that increased AA levels in these lines interferes with root gravitropic responses.

PIN polarity in the stele is altered in* wei2wei7 *and partially rescued by ES8

ES8 has been shown to disturb auxin distribution patterns in the root by altering PIN polarity (Doyle et al., 2015a). Considering that IAA itself can influence its own transport by regulating PIN abundance at the plasma membrane (Paciorek et al., 2005; Robert et al., 2010), we reasoned that AA, as a precursor of IAA, might also play such a role. To investigate this possibility, we first studied the effects of long-term ES8 and AA treatments on the expression pattern of the auxin-responsive promoter *DR5* in the root. To observe the effects of ES8 more easily, we used treatment at a high concentration of 15 µM, which led to a strong decrease in GFP signal in the stele of *DR5::GFP* WT roots (Fig. S7 A), in agreement with previously published work (Doyle et al., 2015a). Furthermore, *DR5::GFP* crossed into the *wei2wei7* background showed a similarly low GFP signal in the stele in control conditions, which was reduced even further by 15 µM ES8 treatment (Fig. S7 A). While 10 µM AA treatment did not noticeably affect the GFP signal in the stele of the WT, the signal in the *wei2wei7* stele was rescued by this treatment (Fig. S7 A). These results suggest that AA may play a role in auxin distribution in the stele.

Next, we focused on the GFP signal in the root tip, particularly around the quiescent center (QC) and in the columella (Fig. S7 B). This time, we treated with ES8 at both 5 and 15 µM concentrations. In agreement with previously published work

(Doyle et al., 2015a), ES8 treatment of *DR5::GFP* WT led to an accumulation of GFP signal in cell file initials surrounding the QC, which were not labeled in control conditions (Fig. S7 B). A rather striking accumulation of *DR5::GFP* signal in the WT, extending into lateral columella and root cap cells, was particularly apparent at the higher ES8 treatment concentration of 15 µM. As found for the stele, *DR5::GFP* crossed into the *wei2wei7* background showed a similar GFP signal pattern in the root tip in control conditions as that induced by ES8 in the WT, with an accumulation of signal in the file initials surrounding the QC (Fig. S7 B). This signal pattern was also apparent in the *wei2wei7* background after 5 µM ES8 treatment and was enhanced after 15 µM ES8 treatment. While 0.5 µM and 10 µM AA treatment did not noticeably affect the GFP signal in the root tip of the WT, the signal pattern in the *wei2wei7* root tip was slightly increased by 0.5 µM AA treatment and rescued to that of the control WT by 10 µM AA treatment (Fig. S7 B). Therefore, in our experiments we observed a negative correlation between the *DR5::GFP* signal strength in the root stele and tip. Together, these results indicate that AA may play a role in auxin distribution in the root stele and tip, which likely affects gravitropic growth.

Our observations of *DR5::GFP* signal in the stele prompted us to investigate the basal to lateral plasma membrane fluorescence ratio (hereafter referred to as basal polarity) of PIN1, PIN3 and PIN7 in the provascular cells of Col-0 and *wei2wei7* root tips. We treated seedlings short-term (2 hours) with 15 µM ES8 or 10 µM AA, performed immunolabeling to observe endogenous PIN1 and PIN7 and used the *PIN3::PIN3-GFP* line crossed into the *wei2wei7* background due to poor labeling of antibodies against PIN3. The fluorescence signals for these PIN proteins were consistently weaker in the mutant than in the WT (Fig. 4 A-C), suggesting decreased abundance of the PIN proteins at the plasma membranes. As previously reported by Doyle et al. (2015a), short-term ES8 treatment significantly, albeit slightly, reduced immunolocalized PIN1 basal polarity in Col-0 and importantly, AA treatment produced a similar result (Fig. 4 D). In contrast, PIN1 basal polarity was significantly increased by about 20% in untreated *wei2wei7* compared to Col-0, while ES8 treatment appeared to rescue this hyper-polarity of PIN1 in the mutant back to almost that of the WT (Fig. 4 D). Although PIN3-GFP basal polarity was not affected by ES8 or AA treatments in either the Col-0 or *wei2wei7* backgrounds, it was increased by over 20% in the mutant

compared to the WT (Fig. 4 E). Finally, although PIN7 basal polarity was not affected by ES8 or AA treatment in Col-0, it was strongly increased in the mutant compared to the WT, and like PIN1, was rescued in the mutant back to the level of the WT by ES8 treatment (Fig. 4 F). These results suggest that AA may play a role in maintenance of PIN polarity in root provascular cells. One possible speculation on why treatment with AA, in contrast to ES8, did not rescue PIN1 or PIN7 polarity in the mutant may be a rapid conversion of AA to downstream IAA precursors within the seedlings.

As AA is a precursor of auxin, which is known to affect transcription of *PIN* genes (Vieten et al., 2005; Paponov et al., 2008), we were interested in the expression levels of these genes in Col-0 and *wei2wei7*. We first investigated gene expression levels for all the plasma membrane-localized PIN proteins (*PIN1*, *PIN2*, *PIN3*, *PIN4* and *PIN7*) in WT and mutant seedlings at nine days old, the age at which we performed our root gravitropic growth and length studies. The expression levels of *PIN1*, *PIN2* and *PIN4* were strongly decreased in *wei2wei7* compared to Col-0, while *PIN3* and *PIN7* expression were somewhat decreased, but not significantly (Fig. S8 A). We next investigated the expression levels of *PIN1*, *PIN3* and *PIN7* in the same conditions used for our PIN polarity studies in root provascular cells (five-day-old seedlings treated with ES8 and AA for 2 hours). At this stage, expression of *PIN1*, *PIN3* and *PIN7* were somewhat decreased in the mutant compared to the WT, but not significantly (Fig. S8 B). Furthermore, treatment with ES8 and AA did not significantly affect the expression of these genes (Fig. S8 B). These results imply that while transcription of *PIN* genes is decreased in *wei2wei7*, the effects of ES8 and AA on PIN polarity are not due to *PIN* gene transcriptional changes. Overall, our data suggest that endogenous AA may play a role in regulating the polarity of PIN1, PIN3 and PIN7 in root provascular cells *via* a mechanism unrelated to *PIN* gene expression levels.

AA regulates root gravitropism* via *repolarization of PIN3 and PIN7 in the columella

Our observations of *DR5::GFP* signal in the columella (Fig. S7 B) indicate that AA may also play a role in auxin distribution specifically in this particular root tissue. Additionally, previous studies of the expression patterns of *ASA1* and *ASB1* promoter-GUS fusions in dark-grown *Arabidopsis* roots revealed strong expression in the root meristem and columella (Stepanova et al., 2005). Plasma membrane-localized PIN3 and

PIN7 in the columella are thought to act in redistribution of auxin in response to gravistimulus (Friml et al., 2002b; Kleine-Vehn et al., 2010), potentially redundantly with PIN4, which is also localized in columella cells (Friml et al., 2002a; Vieten et al., 2005). We therefore reasoned that high expression of anthranilate synthase genes in the columella may reflect a role of AA in regulating gravity-responsive polarity of these PIN proteins. First, to confirm the expression patterns of the *ASA1* and *ASB1* promoters in light-grown roots, we performed GUS staining of *ASA1::GUS* and *ASB1::GUS* seedlings. We observed strong expression of the *ASB1* promoter, but not the *ASA1* promoter, in the stele of the upper root, while neither *ABA1* nor *ASB1* promoter expression was detected in the lower part of the root excluding the root tip (Fig. S9 A and B). Importantly, in agreement with previous studies (Stepanova et al., 2005), we observed strong *ASA1* and *ASB1* promoter expression in the tip of the root meristem and in the columella, with *ASA1::GUS* expressed throughout the columella, while *ASB1::GUS* expression was limited to the innermost columella cells (Fig. S9 C).

Next, we investigated the localization of endogenous PIN3, PIN4 and PIN7 in the columella of Col-0 and *wei2wei7*. Interestingly, we noticed that the fluorescence intensity of these proteins was consistently increased in the innermost cells of the columella in *wei2wei7* compared to Col-0 (Fig. S9 D-F), suggesting that the abundance and/or localization of these proteins are altered in the mutant columella. The antibodies against these PIN proteins did not label the outermost columella cells, in agreement with previous studies using PIN3 and PIN4 antibodies (Friml et al., 2002b; Friml et al., 2002a). We therefore continued our studies of columella PIN proteins using *PIN3::PIN3-GFP* and *PIN7::PIN7-GFP* lines crossed into the *wei2wei7* background (Fig. 5 A and B). We performed long-term treatments of these lines with ES8 and AA and investigated the apical-plus-basal to lateral-plus-lateral fluorescence ratio (hereafter referred to as apical-basal polarity) of the GFP-labeled PIN proteins. Our results revealed that while the apical-basal polarity of PIN3-GFP was similar in *wei2wei7* and Col-0 backgrounds regardless of compound treatment (Fig. 5 C), PIN7-GFP was over 20% more apical-basal polarized in the mutant than in the WT (Fig. 5 D). Moreover, 10 µM AA treatment partially rescued PIN7-GFP polarity in the mutant towards the WT level (Fig. 5 D).

We next investigated gravity-induced relocalization of PIN3-GFP and PIN7-GFP in the columella. After a 90° gravistimulus for 30 minutes, about 15% more PIN3-GFP and PIN7-GFP were present on the now basal (formerly lateral) plasma membranes of the columella cells in WT seedlings (Fig. 5 E and F). Long-term treatment of the WT with 5 µM ES8 or 10 µM AA strongly reduced PIN3-GFP relocalization to only about 5-10% (Fig. 5 E). Strikingly, gravistimulus-induced relocalization of PIN3-GFP was completely absent in mock-treated *wei2wei7*, partially rescued by treatment with 5 µM ES8 and fully rescued by treatment with 10 µM AA (Fig. 5 E). Similar but less pronounced effects were observed for PIN7-GFP in the columella; relocalization was reduced by ES8 in the WT and almost absent in the mock-treated mutant (Fig. 5 F). However, 10 µM AA did not affect PIN7-GFP relocalization in the WT and neither did 5 µM ES8 rescue the relocalization defect in the mutant (Fig. 5 F). The almost total absence of gravistimulus-induced PIN3- and PIN7-GFP relocalization in the *wei2wei7* columella correlates with the mutant's strong agravitropic root phenotype (Fig. 1 C). Moreover, the partial rescue of gravistimulus-induced PIN3-GFP relocalization in *wei2wei7* by long-term treatment with 5 µM ES8 (Fig. 5 F) appears to correlate with the partial rescue of root gravitropic growth by the same treatment (Fig. 1 E). These results imply that endogenous AA may play a role in regulating relocalization of PIN proteins in the columella, especially PIN3, in response to gravity.

To further investigate a potential role for PIN proteins in AA-regulated root gravitropism, we analyzed root gravitropic growth in a range of *pin* mutants and their crosses with *wei2wei7*. Interestingly, while the *eir1-4* (*pin2*) mutant showed intermediate root gravitropic growth between *wei2wei7* and Col-0, crossing these mutants caused an additive effect, with *wei2wei7eir1-4* being more severely agravitropic than *wei2wei7* (Fig. S10 A). Of the tested *pin3*, *pin4* and *pin7* alleles, none of the single mutants were affected in root gravitropic growth compared to the WT and introduction of the *pin3-4* or *pin7-2* mutations into the *wei2wei7* background did not affect the gravitropic growth. Interestingly, in contrast to the *eir1-4* mutation, introduction of the *pin3-5* or *pin4-3* mutations into *wei2wei7* partially rescued the root gravitropic growth compared to *wei2wei7* (Fig. S10 A). While both tested *pin1* alleles showed increased root gravitropic growth compared to the WT, the *pin1-501* mutation

also partially rescued the root gravitropic growth of *wei2wei7* but the *pin1-201* mutation had no effect (Fig. S10 A). The double and triple *pin* mutants tested showed little or no differences in gravitropic growth compared to the WT.

We next tested the effects of long-term treatments with high concentrations of ES8 and AA on root gravitropic growth in the mutants. Most of the tested *pin* mutants showed a similar sensitivity to ES8 as the WT in terms of reduction in root gravitropic growth, except for *eir1-4*, which was more sensitive to ES8 than the WT (Fig. S10 B). Interestingly, although statistically significant differences were not often determined due to large variation in gravitropic index values, introduction of *eir1-4* or either of the *pin1* alleles to the *wei2wei7* background tended to enhance the sensitivity of *wei2wei7* to ES8 (Fig. S10 B). Large variation of gravitropic index values occurred mainly for the most agravitropic samples, due to random directions of root growth. In contrast to *eir1-4* and *pin1*, addition of *pin3, pin4* or *pin7* alleles to *wei2wei7* had no effect on its ES8 sensitivity (Fig. S10 B). In the case of AA treatment, similarly to the WT, none of the *pin* mutants tested showed any sensitivity in terms of changes in root gravitropic growth (Fig. S10 C). While the introduction of *pin3-4* or *pin7-2* to *wei2wei7* did not alter its sensitivity to AA in terms of increase in gravitropic index, crossing *eir1-4* or *pin1-201* into *wei2wei7* significantly increased its sensitivity to AA (Fig. S10 C). In contrast, introduction of *pin3-5*, *pin4-3* or *pin1-501* to *wei2wei7* reduced its sensitivity to AA, resulting in decreased rescue of root gravitropic growth (Fig. S10 C).

In particular, the rescue of, as well as the reduction in AA-induced recovery of, *wei2wei7* root gravitropic growth by introducing *pin1*, *pin3* or *pin4* mutations, provide further evidence for the involvement of PIN1 and PIN3, as well as implicating involvement of PIN4, in AA-regulated root gravitropism. The well-known important role of PIN2 in root gravitropism (Abas et al., 2006; Kleine-Vehn et al., 2008), however, is most likely not related to AA-regulated root gravitropism, considering the strong additive effect of *eir1-4* and *wei2wei7* mutations in reducing root gravitropic growth and increasing sensitivity to both ES8 and AA.

Taken together, our results strongly support a new role for endogenous AA in root gravitropism *via* regulation of selective PIN protein polarity and thereby auxin distribution in both the stele and columella and that this role of AA is independent of its well-known function in IAA biosynthesis.

Discussion

Our work provides strong evidence in favor of a role for AA in root gravitropic growth through regulation of the subcellular localization of auxin transporter proteins, which likely influences the flow of auxin within the organ. The cellular distributions of these proteins are subject to regulation by dynamic and complex endomembrane trafficking. Following their synthesis at the ER, most plasma membrane-targeted proteins are sorted and packaged into selective secretory trafficking routes (Gendre et al., 2014). It has been shown, for instance, that the auxin importer AUXIN-RESISTANT1 (AUX1) and exporter PIN1, when targeted to apical or basal plasma membranes of root tip cells respectively, are transported in distinct endosomes, subject to control by different regulatory proteins (Kleine-Vehn et al., 2006). The trafficking routes of such proteins may be distinct even if targeted to the same plasma membrane. For example, plasma membrane-targeted trafficking pathways for AUX1 and PIN3 in epidermal hypocotyl cells of the apical hook are distinct and subject to different regulatory proteins (Boutté et al., 2013). Such a remarkably complex system of endomembrane trafficking pathways is thought to allow for a high level of control, suggesting the likely existence of an array of selective endogenous compounds and/or signals regulating these trafficking routes.

Once polar plasma membrane-targeted auxin carriers have reached their destination, they remain remarkably dynamic, being subject to constant vesicular cycling (Geldner et al., 2001) to either maintain their localization or rapidly retarget them in response to external stimuli (reviewed by Luschnig and Vert, 2014; and Naramoto, 2017). Auxin itself has been shown to promote its own flow by inhibiting clathrin-mediated endocytosis of PIN transporters, thus enhancing their presence at the plasma membrane (Paciorek et al., 2005). Our results suggest that AA, an important early precursor in the IAA biosynthetic pathways, may also act in a feedback mechanism on PIN plasma membrane localization to regulate the flow of auxin, through currently unknown mechanisms.

The use of pharmacological inhibitors, identified through chemical biology approaches, has proven a powerful strategy that has greatly assisted in unravelling the details of auxin transporter trafficking routes and mechanisms (reviewed by Doyle et al., 2015b; and Hayashi and Overvoorde, 2014). In our previous study, we employed such

a chemical biology strategy, revealing that the AA analog ES8 selectively inhibits an early ER-to-Golgi secretory pathway involved in basal targeting of PIN1 without affecting the polarity of apical plasma membrane proteins (Doyle et al., 2015a). We suggest that AA itself may act endogenously on trafficking regulation in a similar way to ES8 and it will be interesting to investigate this possibility in follow-up studies. As ES8 appears to mimic the effects of AA on PIN localization and root gravitropic growth, without releasing AA through degradation and without affecting IAA levels, this synthetic compound has proven extremely useful for dissecting this newly discovered role of AA from its better-known role in auxin biosynthesis.

Interestingly, the amino acid para-aminobenzoic acid, which has a similar structure to AA and is produced from the same precursor, has also recently been shown to play a role in root gravitropism, distinct from its better known role in folate biosynthesis (Nziengui et al., 2018). However, unlike AA, para-aminobenzoic acid promotes gravitropic root growth in wild type plants as well as promoting gravistimulated root bending by enhancing the asymmetric auxin response between the two root sides (Nziengui et al., 2018). AA is an important endogenous compound in plants, functioning as an early precursor in the chloroplast-localized biosynthetic pathway producing the amino acid tryptophan (Maeda and Dudareva, 2012). Tryptophan is itself an essential amino acid, acting as a precursor for several indole-containing plant compounds, including IAA, the predominant auxin in plant tissues (Mano and Nemoto, 2012). Our strategy to simultaneously overexpress and silence *ASA1* and *PAT1*, respectively, resulted in increased AA levels within the transformed plant tissues, without affecting the IAA content. While this proved to be very effective for separating the role of AA in auxin biosynthesis from root gravitropic responses, which we suggest are rather regulated by a role of AA in PIN localization, one might have expected that lowered levels of PAT1, an important enzyme for Trp biosynthesis, should lead to lowered downstream IAA content. However, our analysis of IAA conjugates and catabolites in these lines revealed dramatically reduced IAAsp content and somewhat reduced oxIAA content, highlighting the well-documented importance of IAA conversion to these compounds in maintaining the required balance of bioactive auxin within tissues (reviewed by Korasick et al., 2013). A family of GRETCHEN HAGEN 3 (GH3) IAA-amido synthetases conjugate IAA to several amino acids

(Staswick et al., 2005), while two DEOXYGENASE FOR AUXIN OXIDATION (DAO) enzymes have recently been identified in *Arabidopsis* (Porco et al., 2016), with DAO1 specifically demonstrated to catalyze oxIAA (Zhang et al., 2016). These enzymes are thought to be extremely important in regulating auxin homeostasis by converting IAA to inactive and storage forms (reviewed by Zhang and Peer, 2017).

The agravitropic growth of *wei2wei7* roots may be due to a combination of decreased auxin content caused by reduced AA levels and the AA deficiency itself, as both auxin and AA affect the localization and polarity of PIN proteins. As was shown previously for ES8 (Doyle et al., 2015a), AA appears to act selectively depending on the PIN protein and the root tissue. PIN1, PIN3 and PIN7 all display increased basal polarity in provascular cells of *wei2wei7* compared to Col-0, suggesting increased flow of auxin towards the root tip in the mutant. Correspondingly, we found decreased expression of the auxin-responsive promoter *DR5* in the root stele and increased expression around the root tip QC in the mutant, a pattern that was also observed in WT roots upon ES8 treatment. PIN7, but not PIN3, is also abnormally polarized in columella cells of *wei2wei7*, while both these proteins appear to be completely unresponsive to gravitropic stimulus in the mutant columella. Furthermore, the high expression of *ASA1* and *ASB1* in the root columella of the WT suggests the importance of AA in this tissue in particular, which our results suggest is due to a role for this compound in gravity-regulated PIN distribution on the plasma membranes. The particular importance of PIN1 and PIN3 in AA-regulated root gravitropism was further supported by the rescue, as well as the reduction in AA-induced rescue, of *wei2wei7* root gravitropic growth by introduction of *pin1* or *pin3* mutations.

Taken together, our results strongly suggest that the endogenous compound AA plays a role in root gravitropism by regulating the polarity and gravity-induced relocalization of specific PIN proteins in the provascular and columella cells. Furthermore, this role of AA is distinct from its well-known function in auxin biosynthesis, which we suggest is more important for root elongation than gravitropic growth.

Materials and Methods

Plant material and growth conditions

For surface sterilization of *Arabidopsis thaliana* seeds, one tablet of Bayrochlor (Bayrol) was dissolved in 40 ml distilled water before diluting 1:10 in 95% ethanol. Seeds were then incubated in the Bayrochlor solution (active ingredient sodium dichloroisocyanurate) for 6 min followed by two rinses with 95% ethanol. Seeds were then allowed to dry in a sterile environment before sowing on plates of growth medium containing ½ strength Murashige and Skoog (MS) medium at pH 5.6 with 1% sucrose, 0.05% MES and 0.7% plant agar (Duchefa Biochemie). Two d after stratification at 4°C to synchronize germination, the plates were positioned vertically and the seedlings were grown for 5 or 9 d at 22 °C on a 16 h : 8 h light : dark photoperiod. The Columbia-0 (Col-0) accession was used as the WT except for growth of *pin3-5pin4-3pin7-1* seedlings, for which the Landsberg *erecta* (L*er*) accession was also used, being the background for the *pin7-1* allele. See Table S1 for the previously published *Arabidopsis* lines used. All mutants and marker lines in the *wei2wei7* background were generated in this study by crossing. For selection of homozygous lines at the F2 generation, seedlings displaying a *wei2wei7* phenotype were initially selected and then genotyped for the third mutation for triple mutants (see Table S2 for primers used), or observed on a fluorescence stereomicroscope for GFP marker line crosses. Finally, selected lines were confirmed for homozygous *wei2-1* and *wei7-1* mutations by genotyping (see Table S2 for primers used). The heterozygous lines *pin1-201* and *pin1-501* (we added *01* to the name of this mutant to distinguish from another *pin1-5* allele) and their crosses with *wei2wei7* were transferred to soil after imaging on treatment plates and only those that later formed pin-like inflorescences were included in root measurements in the initial images. All root length and gravitropic index measurements were performed on 9-d-old seedlings, while microscopy studies were performed on 5-d-old seedlings due to cell collapse in a proportion of the tips of older *wei2wei7* roots. ImageJ software (https://imagej.nih.gov/ij/) was used to measure root length and vertical gravitropic index, which was calculated for each root as a ratio of L_y : L, where L_y is the vertical distance from root base to tip, or the real depth of root tip penetration, and L is the root length, as described in Grabov et al. (2005). For gravistimulated root bending experiments, seedlings were grown vertically for 5 d in treatment-free conditions, then

transferred to mock or estradiol-supplemented medium for 24 h, and then gravistimulated by turning the plates 90° for 24 h before measuring the root bending angles. The angles were measured in the direction of root bending between two lines intersecting at the former root tip position before gravistimulus, one being horizontal and the other originating from the current root tip position (Fig. S6 D).

Chemical treatments

Stock solutions of ES8 (ID 6444878; Chembridge), AA (Sigma-Aldrich), ES8.7 (ID 6437223; Chembridge) and ES8.7-Trp (see *Chemical synthesis*) were made in DMSO. Chemicals were diluted in liquid medium for short-term treatments (2 h) or growth medium for long-term treatments (5 or 9 d), in which case seeds were directly sown and germinated on chemical-supplemented medium. Equal volumes of solvent were used as mock treatments for controls. For live imaging, seedlings were mounted in their treatment medium for microscopic observations.

IAA metabolite analysis

For quantification of endogenous IAA and its metabolites, 20-30 whole seedlings per sample were flash-frozen in liquid nitrogen and ground with plastic microtube pestles. Approximately 20 mg of ground tissue was collected per sample and stored at -80^{o}C. Extraction and analysis were performed according to Novák et al. (2012). Briefly, frozen samples were homogenized using a MixerMill bead mill (Retsch GmbH) and extracted in 1 ml of 50 mM sodium phosphate buffer containing 1% sodium diethyldithiocarbamate and a mixture of $^{13}C_6$- or deuterium-labeled internal standards. After pH adjustment to 2.7 by 1 M HCl, a solid-phase extraction was performed using Oasis HLB columns (30 mg 1 cc; Waters). Mass spectrometry analysis and quantification were performed by a liquid chromatography–tandem mass spectrometry (LC-MS/MS) system comprising of a 1290 Infinity Binary LC System coupled to a 6490 Triple Quad LC/MS System with Jet Stream and Dual Ion Funnel technologies (Agilent Technologies).

Chemical synthesis

The following procedure was used to synthesize (4-(*N*-(4-chlorobenzyl) methylsulfonamido)benzoyl)tryptophan (ES8.7-Trp). Methyl sulfonyl chloride (3.1 ml, 45.5 mmol, 1.2 equivalent) and pyridine (3 ml, 37.1 mmol, 1.1 equivalent) were added to a solution of 4-aminoethylbenzoate (5.1 g, 33.7 mmol) in acetonitrile (100 ml) at 0°C and then stirred overnight at room temperature. The reaction mixture was concentrated and the resulting residue was dissolved in ethyl acetate. The organic layer was washed with HCl (2 *N*, 100 ml), saturated $NaHCO_3$, H_2O and brine, dried over Na_2SO_4, and concentrated to give an off-white solid (7.1 g, 94%), ethyl 4-(methylsulfonamido) benzoic acid, which was used without further purification. Then 4-chlorobenzyl bromide (1.43 ml, 11 mmol, 1.2 equivalent) and K_2CO_3 (3.8 g, 27.4 mmol, 3 equivalent) were added to a solution of ethyl 4-(methylsulfonamido)benzoate (2.1 g, 9.15 mmol) in dimethylformamide (DMF) (14 ml). The reaction mixture was stirred overnight after which liquid chromatography-mass spectrometry indicated the reaction was complete, yielding 4-(*N*-(4-chlorobenzyl)methylsulfonamido)ethylbenzoate (2.8 g, 88%). Next, NaOH (2 *N*, 15 ml) and H_2O (10 ml) were added to 2 g of 4-(*N*-(4-chlorobenzyl)methylsulfonamido)ethylbenzoate, followed by overnight stirring. The reaction mixture was acidified to pH 5 with concentrated HCl and partitioned between ethyl acetate and H_2O. The organic layer was washed with brine, dried over Na_2SO_4, and concentrated to give 4-(*N*-(4-chlorobenzyl)methylsulfonamido)ethylbenzoate (1.7 g, 92%), which was used without further purification. Then 10 ml thionyl chloride was added to a solution of 1 mmol 4-(*N*-(4-chlorobenzyl)methylsulfonamido)ethylbenzoate and refluxed for 12 h under a nitrogen atmosphere. The thionyl chloride was removed under reduced pressure to give acid chloride. Then 1.2 mmol tryptophan was dissolved in 5 ml DMF and cooled to 0°C. At this temperature the acid chloride was added slowly by dissolving in 3 ml DMF. The reaction mixture was stirred at room temperature for 24 h. Ice cold water was added to the reaction mixture, which was then extracted with chloroform and washed with brine solution three times to afford the crude mixture. Finally, purification with column chromatography using methanol and chloroform as a solvent system resulted in a light yellow solid, (4-(*N*-(4-chlorobenzyl) methylsulfonamido)benzoyl)tryptophan (ES8.7-Trp) with 68% yield.

Compound degradation analysis

For short-term treatments with 5 µM ES8 compounds, 5-day-old Col-0 and *wei2wei7* seedlings were incubated for 5 h in ES8, ES8.7 and ES8.7-Trp-supplemented liquid medium before harvesting in liquid nitrogen along with samples of liquid treatment medium incubated for 5 h without any seedlings. For long-term treatments with 5 µM ES8 compounds, Col-0 and *wei2wei7* seedlings were grown for 9 days on ES8, ES8.7 and ES8.7-Trp-supplemented solid medium before harvesting in liquid nitrogen along with samples of solid treatment medium incubated for 9 days without any seedlings. Samples from two biological replicates were harvested and divided into two technical replicates each. The medium samples were diluted 1:100 with 30% v/v acetonitrile and 10 µl was injected onto a Kinetex 1.7 µm C18 100A reversed-phase column 50 x 2.1 mm (Phenomenex) followed by analysis by LC-MS/MS. The seedling samples (around 10 mg fresh weight) were extracted in 0.4 ml acetonitrile using a MixerMill MM 301 bead mill (Retsch GmbH) with 2 mm ceria-stabilized zirconium oxide beads at a frequency of 27 Hz for 3 min. The plant tissue extracts were then incubated at 4°C with continuous shaking for 30 min, centrifuged in a Beckman Coulter Avanti 30 at 4°C for 15 min at 36,670 *g* and purified by liquid-liquid extraction using acetonitrile:hexan:H_2O:formic acid (4:5:1:0.01) to remove impurities and the sample matrix. After 30 min incubation at 4°C, the acetonitrile fractions were removed, evaporated to dryness *in vacuo* and dissolved in 50 µl 30% v/v acetonitrile prior to LC-MS/MS analysis using an Acquity UPLC I-Class System (Waters) coupled to a Xevo TQ-S MS triple quadrupole mass spectrometer (Waters). After injection of 10 µl, the purified samples were eluted using an 11 min gradient comprised of 0.1% acetic acid in methanol (A) and 0.1% acetic acid in water (B) at a flow rate of 0.5 ml/min and column temperature of 40°C. The binary linear gradient of 0 min 2:98 A:B, 11 min 95:5 A:B was used, after which the column was washed with 100% methanol for 1 min and re-equilibrated to initial conditions for 2 min. The effluent was introduced into the MS system with the following optimal settings: source/desolvation temperature 150/600°C, cone/desolvation gas flow 150/1000 L/h, capillary voltage 1 kV, cone voltage 25-40 V, collision energy 15-30 eV and collision gas flow (argon) 0.21 ml/min. Quantification and confirmation of the ES8 compounds were obtained by the multiple reaction monitoring mode using the following mass transitions: 274>111/274>230,

457>378/457>413 and 526>125/526>322 for ES8, ES8.7 and ES8.7-Trp, respectively. The non-AA and non-Trp parts of the ES8 compounds were monitored by high resolution mass spectrometry (HRMS) using a Synapt G2-Si hybrid Q-TOF tandem mass spectrometer (Waters) equipped with electrospray ionization (ESI) interface (source temperature 150°C, desolvation temperature 550°C, capillary voltage 1 kV and cone voltage 25 V). Nitrogen was used as the cone gas (50 L/h) and the desolvation gas (1000 L/h). Data acquisition was performed in full-scan mode (50-1000 Da) with a scan time of 0.5 sec and collision energy of 4 eV; argon was used as the collision gas (optimized pressure of 5 x 10^{-3} mbar). The HRMS analyses were performed in positive (ESI^+) and negative (ESI^-) modes. Finally, analyses of AA and Trp were performed according to Novák et al. (2012) (see *IAA metabolite analysis*). All chromatograms were analyzed with MassLynx software (version 4.1; Waters) and the compounds were quantified according to their recovery.

Generation of* 35S::ASA1 *and* XVE::amiRNA-PAT1 *lines

See Table S2 for primers used. For constitutive overexpression of *ASA1* (AT5G05730), the coding region of the gene was amplified from *Arabidopsis thaliana* Col-0 cDNA. Primers for artificial microRNA (amiRNA) to knock down the *PAT1* (AT5G17990) gene were designed using the Web MicroRNA Designer tool (http://wmd3.weigelworld.org). The amiRNA was obtained using the pRS300 vector as a PCR template, as described previously (Ossowski et al., 2008). The fragments were introduced into the Gateway pENTR/D-TOPO cloning vector (Invitrogen) and verified by sequencing. The *ASA1* coding sequence was then cloned into the DL-phosphinothricin-resistant vector pFAST-R02 (Shimada et al., 2010), while the amiRNA was cloned into the hygromycin-resistant vector pMDC7b containing the estradiol-inducible XVE system (Curtis and Grossniklaus, 2003), using the LR reaction (Invitrogen). *Agrobacterium*-mediated transformation of the constructs into *Arabidopsis thaliana* Col-0 was achieved by floral dipping (Clough and Bent, 1998). Transformed plants were selected *via* antibiotic resistance on agar plates supplied with the respective antibiotics, 50 µg ml^{-1} hygromycin B or 25 µg ml^{-1} DL-phosphinothricin. Four and six independent homozygous *35S::ASA1* and *XVE::amiRNA-PAT1* lines were analyzed, respectively. Two lines per construct were then selected that displayed strong and

reproducible constitutive *ASA1* induction or induced *PAT1* silencing, as determined by performing qPCR (see *Quantitative PCR*) using RNA extracted from one-week-old whole seedlings (Fig. S6 A and B). To induce silencing in the *XVE::amiRNA-PAT1* seedlings, the seedlings were germinated and grown on agar plates supplemented with 20 µM estradiol, with DMSO used as a mock treatment control. Each selected *35S::ASA1* line was crossed with each selected *XVE::amiRNA-PAT1* line and homozygous F2 generation offspring, named *AxP* (*ASA1 x PAT1*) lines, were selected as before *via* antibiotic resistance. The homozygous lines were then tested for gene expression as before *via* qPCR (12 independent lines were analyzed) (Fig. S6 C and D). Finally, two lines displaying reproducible simultaneous constitutive *ASA1* induction and induced *PAT1* silencing were selected for use in further experiments.

Quantitative PCR

Total RNA was extracted from whole seedlings using the RNeasy Plant Mini Kit (Qiagen) according to the manufacturer's instructions. Samples were harvested in liquid nitrogen and the frozen tissue ground directly in their microtubes using microtube pestles. RQ1 RNase-free DNase (Promega) was used for the on-column DNase digestion step. RNA concentration was measured with a NanoDrop 2000 spectrophotometer (Thermo Scientific). cDNA was prepared with 1 µg RNA using the iScript cDNA Synthesis Kit (Bio-Rad) according to the manufacturer's instructions. Serial dilutions of pooled cDNA from all samples for a particular experiment were used to determine efficiencies for each primer pair. Quantitative real-time PCR was performed on a LightCycler 480 System (Roche Diagnostics) using LightCycler 480 SYBR Green I Master reagents (Roche Diagnostics), including 2 technical replicates per sample. For amplification of mRNA, the following protocol was applied: 95^{o}C for 5 min, then 40 cycles of 95^{o}C for 10 sec, 60^{o}C for 15 sec and 72^{o}C for 20 sec. For each experiment, transcriptional levels of the four reference genes AT5G25760, AT1G13440, AT4G34270 and AT1G13320 were analyzed alongside the target genes (see Table S2 for primers used). Expression levels of the target genes were normalized against the two most stably expressed reference genes, as determined using GeNorm (Biogazelle) (Vandesompele et al., 2002), using the formula below, where E = efficiency, R =

reference gene, Cq = quantification cycle mean, T = target gene. For each target gene, the normalized expression values were scaled relative to that of the WT control.

Normalized expression = $\sqrt{(ER1^{CqR1} + ER2^{CqR2})} \Big/ ET^{CqT}$

Generation of PIN7 antibody

For the generation of anti-PIN7, a region of 882 bp corresponding to the hydrophilic loop of PIN7 was amplified and attB1 and attB2 recombination sites were incorporated (see Table S2 for primer sequences). The amplicon was recombined into the pDONR221 vector (Invitrogen) and the resulting pDONR221::PIN7HL was recombined into the pDEST17 vector (Invitrogen) in order to express the PIN7HL (31.4 kDa) in BL21 DE Star A *E. coli* cells. Cell cultures (250 ml) were induced in the logarithmic stage (after approx. 3.5 h) with 0.5 mM isopropyl β-D-1-thiogalactopyranoside (IPTG) for 7 h. Cells were harvested by centrifugation and resuspended in 15 ml PBS at pH 8.0 with 8 M urea and 10 mM imidazole and incubated at 4°C for 2 d. The PIN7HL expressed peptide was purified according to the Ni-NTA Purification System (Qiagen). The purified protein was then diluted in PBS buffer at pH 8.0 and desalted using Thermo Scientific Pierce concentrators 9K MWCO. The concentrated peptide was once more diluted in PBS at pH 8.0 before antibody production in rabbit, which was performed by the Moravian Biotechnology company (http://www.moravian-biotech.com/). Finally, serum specificity tests were performed in Col-0, *pin7* mutants and *PIN7-GFP* lines.

Immunolocalization and confocal microscopy

Immunolocalization in *Arabidopsis* roots was performed as described previously, using an Intavis InsituPro Vsi (Doyle et al., 2015a). Primary antibodies used were anti-PIN1 at 1:500 (NASC), anti-PIN3 at 1:150 (NASC), anti-PIN4 at 1:400 (NASC) and anti-PIN7 at 1:600. Secondary antibodies used were Cy3-conjugated anti-rabbit and anti-sheep at 1:400 and 1:250, respectively (Jackson ImmunoResearch). Confocal laser scanning microscopy on seedling root tips was performed using a Zeiss LSM 780 confocal microscope with 40X water-immersion objective lens and images were acquired with Zeiss ZEN software using identical acquisition parameters between mock and chemical treatments and between the WT and mutant in each experiment. For PIN

basal polarity index quantification in provascular cells, the 'mean gray area' tool in ImageJ was used to measure plasma membrane fluorescence intensity in confocal images and a basal (lower) to lateral fluorescence ratio was calculated for each cell measured. To monitor gravitropically induced PIN relocalization in root columella cells, confocal Z-scans were acquired before and 30 min after gravistimulation, during which the seedlings were rotated 90° to the horizontal position. Fluorescence intensity at the apical (upper), basal (lower) and lateral plasma membranes of the cells was measured on maximal intensity projections of the Z-scans using ImageJ. For PIN apicl-basal polarity index measurements, the apical-plus-basal to lateral-plus-lateral fluorescence ratio was calculated. For PIN relocalization measurements, the signal intensity ratio between the outermost lateral plasma membranes on the periphery of the columella (left and right sides) was measured before and after gravistimulation and these ratios were compared.

GUS staining

Seedlings were fixed in 80% acetone at -20°C for 20 min, washed three times with distilled water and then incubated in 2 mM X-GlcA in GUS buffer (0.1% triton X100, 10 mM EDTA, 0.5 mM potassium ferrocyanide and 0.5 mM potassium ferricyanide in 0.1 M phosphate buffer (Na2HPO4 / NaH2PO4) at pH 7). The samples were then infiltrated for 10 min in a vacuum desiccator before incubation in the dark at 37°C. The GUS reaction was stopped by replacing the GUS buffer with 70% ethanol. Samples were then mounted in 50% glycerol and observed on a Zeiss Axioplan microscope.

Statistical analyses

For all experiments, at least 3 biological replicates were performed and always on different days. When more than 3 or 4 biological replicates were performed, this was due to poor growth of *wei2wei7* that occasionally resulted in a low number of seedlings or quantifiable roots in some of the replicates. Wilcoxon rank sum (Mann–Whitney U) tests or Student's t-tests were performed on full, raw datasets of nonparametric or parametric data, respectively, to determine statistically significant differences. On all charts, the means and standard errors of the biological replicates are displayed.

Supplemental material

Ten supplementary figures and two supplementary tables accompany this article.

Acknowledgments

The authors declare no competing financial interests. We acknowledge the Knut and Alice Wallenberg Foundation (F. Almqvist), in particular the KAW "ShapeSystems" grant number 2012.0050 (S. M. Doyle., M. Karady, K. Ljung and S. Robert), the Plant Fellows fellowship program (A. Rigal), the Swedish Research Council (F. Almqvist), in particular the SRC and Vinnova grants VR2003-4632 (M. Majda) and VR2016-00768 (P. Grones), the Kempe (F. Almqvist and P. Grones) and Carl Tryggers (P. Grones) Foundations, the Ghent University Special Research Fund (M. Karampelias), the Czech Science Foundation project no. 13-40637S (M. Zwiewka), the Göran Gustafsson Foundation (F. Almqvist) and the Swedish Foundation for Strategic Research (F. Almqvist) for funding. The core facility CELLIM of CEITEC was supported by the MEYS CR (LM2015062 Czech-BioImaging). We are grateful to Vanessa Schmidt and Roger Granbom for technical assistance. We gratefully thank Christian Luschnig and Jiří Friml for sharing seeds and antibodies and Per-Anders Enquist for technical advice. We are especially grateful to Hélène S. Robert for sharing antibodies and primer sequences, for helpful advice and for critical reading of the manuscript. We acknowledge the Nottingham Arabidopsis Stock Centre (NASC) for distributing seeds and the many colleagues who kindly shared published *Arabidopsis* lines with us.

Author contributions

Siamsa M. Doyle, Adeline Rigal and Stéphanie Robert conceived and designed the research; Siamsa M. Doyle, Adeline Rigal, Peter Grones, Michal Karady, Deepak K. Barange, Mateusz Majda, Barbora Pařízková, Aleš Pěnčik and Ondřej Novák performed the experiments; Michael Karampelias and Marta Zwiewka produced and tested the PIN7 antibody; Fredrik Almqvist, Karin Ljung, Ondřej Novák and Stéphanie Robert supervized the research; Siamsa M. Doyle wrote the article with feedback from all the authors.

References

Abas, L., R. Benjamins, N. Malenica, T. Paciorek, J. Wiśniewska, J. C. Moulinier-Anzola, T. Sieberer, J. Friml, and C. Luschnig. 2006. Intracellular trafficking and proteolysis of the *Arabidopsis* auxin-efflux facilitator PIN2 are involved in root gravitropism. *Nat Cell Biol,* 8**,** 249-56.

Adamowski, M., and J. Friml. 2015. PIN-dependent auxin transport: action, regulation, and evolution. *Plant Cell,* 27**,** 20-32.

Boutté, Y., K. Jonsson, H. E. Mcfarlane, E. Johnson, D. Gendre, R. Swarup, J. Friml, L. Samuels, S. Robert, and R. P. Bhalerao. 2013. ECHIDNA-mediated post-Golgi trafficking of auxin carriers for differential cell elongation. *Proc Natl Acad Sci U S A.*

Clark, N. M., M. A. De Luis Balaguer, and R. Sozzani. 2014. Experimental data and computational modeling link auxin gradient and development in the Arabidopsis root. *Front Plant Sci*, 5**,** 328.

Clough, S. J., and A. F. Bent. 1998. Floral dip: a simplified method for Agrobacterium-mediated transformation of Arabidopsis thaliana. *Plant J,* 16**,** 735-43.

Curtis, M. D., and U. Grossniklaus. 2003. A gateway cloning vector set for high-throughput functional analysis of genes in planta. *Plant Physiol,* 133**,** 462-9.

Doyle, S. M., A. Haeger, T. Vain, A. Rigal, C. Viotti, M. Łangowska, Q. Ma, J. Friml, N. V. Raikhel, G. R. Hicks, and S. Robert. 2015a. An Early Secretory Pathway Mediated by GNOM-LIKE 1 and GNOM is Essential for Basal Polarity Establishment in *Arabidopsis thaliana*. *Proc Natl Acad Sci U S A,* 112**,** E806-E815.

Doyle, S. M., T. Vain, and S. Robert. 2015b. Small molecules unravel complex interplay between auxin biology and endomembrane trafficking. *J Exp Bot,* 66**,** 4971-4982.

Friml, J., E. Benková, I. Blilou, J. Wisniewska, T. Hamann, K. Ljung, S. Woody, G. Sandberg, B. Scheres, G. Jürgens, and K. Palme. 2002a. AtPIN4 mediates sink-driven auxin gradients and root patterning in *Arabidopsis*. *Cell,* 108**,** 661-673.

Friml, J., J. Wiśniewska, E. Benková, K. Mendgen, and K. Palme. 2002b. Lateral relocation of auxin efflux regulator PIN3 mediates tropism in *Arabidopsis*. *Nature,* 415**,** 806-809.

Geisler, M., B. Wang, and J. Zhu. 2014. Auxin transport during root gravitropism: transporters and techniques. *Plant Biol (Stuttg),* 16 Suppl 1**,** 50-7.

Geldner, N., J. Friml, Y.-D. Stierhof, G. Jürgens, and K. Palme. 2001. Auxin transport inhibitors block PIN1 cycling and vesicle trafficking. *Nature,* 413**,** 425-428.

Gendre, D., K. Jonsson, Y. Boutté, and R. P. Bhalerao. 2014. Journey to the cell surface-the central role of the trans-Golgi network in plants. *Protoplasma,* 252**,** 385-398.

Goh, T., U. Vobeta, E. Farcot, M. J. Bennett, and A. Bishopp. 2014. Systems biology approaches to understand the role of auxin in root growth and development. *Physiol Plant,* 151**,** 73-82.

Grabov, A., M. K. Ashley, S. Rigas, P. Hatzopoulos, L. Dolan, and F. Vicente-Agullo. 2005. Morphometric analysis of root shape. *New Phytol,* 165**,** 641-51.

Hayashi, K., and P. Overvoorde. 2014. Use of Chemical Biology to Understand Auxin Metabolism, Signaling, and Polar Transport. *In:* AUDENAERT, D. & OVERVOORDE, P. (eds.) *Plant Chemical Biology.* Wiley.

Ikeda, Y., S. Men, U. Fischer, A. N. Stepanova, J. M. Alonso, K. Ljung, and M. Grebe. 2009. Local auxin biosynthesis modulates gradient-directed planar polarity in *Arabidopsis*. *Nat Cell Biol,* 11**,** 731-8.

Kleine-Vehn, J., P. Dhonukshe, R. Swarup, M. Bennett, and J. Friml. 2006. Subcellular trafficking of the *Arabidopsis* auxin influx carrier AUX1 uses a novel pathway distinct from PIN1. *Plant Cell,* 18**,** 3171-3181.

Kleine-Vehn, J., Z. Ding, A. R. Jones, M. Tasaka, M. T. Morita, and J. Friml. 2010. Gravity-induced PIN transcytosis for polarization of auxin fluxes in gravity-sensing root cells. *Proc Natl Acad Sci U S A,* 107**,** 22344-22349.

Kleine-Vehn, J., J. Leitner, M. Zwiewka, M. Sauer, L. Abas, C. Luschnig, and J. Friml. 2008. Differential degradation of PIN2 auxin efflux carrier by retromer-dependent vacuolar targeting. *Proc Natl Acad Sci U S A,* 105**,** 17812-7.

Korasick, D. A., T. A. Enders, and L. C. Strader. 2013. Auxin biosynthesis and storage forms. *J Exp Bot,* 64**,** 2541-55.

Ljung, K. 2013. Auxin metabolism and homeostasis during plant development. *Development,* 140**,** 943-50.

Luschnig, C., and G. Vert. 2014. The dynamics of plant plasma membrane proteins: PINs and beyond. *Development,* 141**,** 2924-2938.

Maeda, H., and N. Dudareva. 2012. The shikimate pathway and aromatic amino acid biosynthesis in plants. *Annu Rev Plant Biol,* 63**,** 73-105.

Mano, Y., and K. Nemoto. 2012. The pathway of auxin biosynthesis in plants. *J Exp Bot,* 63**,** 2853-72.

Müller, A., C. Guan, L. Gälweiler, P. Tänzler, P. Huijser, A. Marchant, G. Parry, M. Bennett, E. Wisman, and K. Palme. 1998. *AtPIN2* defines a locus of *Arabidopsis* for root gravitropism control. *EMBO J,* 17**,** 6903-11.

Naramoto, S. 2017. Polar transport in plants mediated by membrane transporters: focus on mechanisms of polar auxin transport. *Curr Opin Plant Biol,* 40**,** 8-14.

Niyogi, K. K., and G. R. Fink. 1992. Two anthranilate synthase genes in Arabidopsis: defense-related regulation of the tryptophan pathway. *Plant Cell,* 4**,** 721-33.

Novák, O., E. Hényková, I. Sairanen, M. Kowalczyk, T. Pospíšil, and K. Ljung. 2012. Tissue-specific profiling of the *Arabidopsis thaliana* auxin metabolome. *Plant J,* 72**,** 523-36.

Nziengui, H., H. Lasok, P. Kochersperger, B. Ruperti, F. Rebeille, K. Palme, and F. A. Ditengou. 2018. Root gravitropism is regulated by a crosstalk between para-aminobenzoic acid, ethylene, and auxin. *Plant Physiol*.

Ossowski, S., R. Schwab, and D. Weigel. 2008. Gene silencing in plants using artificial microRNAs and other small RNAs. *Plant J,* 53**,** 674-90.

Paciorek, T., E. Zažímalová, N. Ruthardt, J. Petrášek, Y.-D. Stierhof, J. Kleine-Vehn, D. A. Morris, N. Emans, G. Jürgens, N. Geldner, and J. Friml. 2005. Auxin inhibits endocytosis and promotes its own efflux from cells. *Nature,* 435**,** 1251-1256.

Paponov, I. A., M. Paponov, W. Teale, M. Menges, S. Chakrabortee, J. A. Murray, and K. Palme. 2008. Comprehensive transcriptome analysis of auxin responses in Arabidopsis. *Mol Plant,* 1**,** 321-37.

Porco, S., A. Pencik, A. Rashed, U. Voss, R. Casanova-Saez, A. Bishopp, A. Golebiowska, R. Bhosale, R. Swarup, K. Swarup, P. Penakova, O. Novak, P. Staswick, P. Hedden, A. L. Phillips, K. Vissenberg, M. J. Bennett, and K.

Ljung. 2016. Dioxygenase-encoding AtDAO1 gene controls IAA oxidation and homeostasis in Arabidopsis. *Proc Natl Acad Sci U S A,* 113**,** 11016-21.

Robert, S., J. Kleine-Vehn, E. Barbez, M. Sauer, T. Paciorek, P. Baster, S. Vanneste, J. Zhang, S. Simon, M. Čovanová, K. Hayashi, P. Dhonukshe, Z. Yang, S. Y. Bednarek, A. M. Jones, C. Luschnig, F. Aniento, E. Zažímalová, and J. Friml. 2010. ABP1 mediates auxin inhibition of clathrin-dependent endocytosis in *Arabidopsis*. *Cell,* 143**,** 111-121.

Rose, A. B., A. L. Casselman, and R. L. Last. 1992. A phosphoribosylanthranilate transferase gene is defective in blue fluorescent *Arabidopsis thaliana* tryptophan mutants. *Plant Physiol,* 100**,** 582-92.

Shimada, T. L., T. Shimada, and I. Hara-Nishimura. 2010. A rapid and non-destructive screenable marker, FAST, for identifying transformed seeds of Arabidopsis thaliana. *Plant J,* 61**,** 519-28.

Staswick, P. E., B. Serban, M. Rowe, I. Tiryaki, M. T. Maldonado, M. C. Maldonado, and W. Suza. 2005. Characterization of an Arabidopsis enzyme family that conjugates amino acids to indole-3-acetic acid. *Plant Cell,* 17**,** 616-27.

Stepanova, A. N., J. M. Hoyt, A. A. Hamilton, and J. M. Alonso. 2005. A Link between ethylene and auxin uncovered by the characterization of two root-specific ethylene-insensitive mutants in Arabidopsis. *Plant Cell,* 17**,** 2230-42.

Vandesompele, J., K. De Preter, F. Pattyn, B. Poppe, N. Van Roy, A. De Paepe, and F. Speleman. 2002. Accurate normalization of real-time quantitative RT-PCR data by geometric averaging of multiple internal control genes. *Genome Biol,* 3**,** research34.

Vanneste, S., and J. Friml. 2009. Auxin: a trigger for change in plant development. *Cell,* 136**,** 1005-1016.

Vieten, A., S. Vanneste, J. Wisniewska, E. Benkova, R. Benjamins, T. Beeckman, C. Luschnig, and J. Friml. 2005. Functional redundancy of PIN proteins is accompanied by auxin-dependent cross-regulation of PIN expression. *Development,* 132**,** 4521-31.

Zhang, J., J. E. Lin, C. Harris, F. Campos Mastrotti Pereira, F. Wu, J. J. Blakeslee, and W. A. Peer. 2016. DAO1 catalyzes temporal and tissue-specific oxidative inactivation of auxin in Arabidopsis thaliana. *Proc Natl Acad Sci U S A,* 113**,** 11010-5.

Zhang, J., and W. A. Peer. 2017. Auxin homeostasis: the DAO of catabolism. *J Exp Bot,* 68**,** 3145-3154.

Zhao, Y. 2014. Auxin biosynthesis. *Arabidopsis Book,* 12**,** e0173.

Figure Legends

Figure 1. AA rescues root gravitropic growth and length differently in an AA-deficient mutant. (A) Chemical structures of ES8 and AA. **(B)** Root gravitropic index and length in 9-day-old Col-0 and *wei2wei7* seedlings. **(C)** Representative images of 9-day-old Col-0 and *wei2wei7* seedlings grown on treatment-supplemented medium. Scale bar represents 1 cm. **(D-E)** Root gravitropic index and length in 9-day-old seedlings of *wei2wei7* grown on medium supplemented with a range of concentrations of AA (D) or

ES8 (E). Asterisks indicate samples significantly different from Col-0 (B) or the mock-treated control (D-E) (***p<0.001, *p<0.05). Error bars indicate standard error of the mean of the biological replicates. Values in square brackets indicate treatment concentrations in µM. *n* = 25 seedlings per sample per each of 4 (B), 3 (D) or 6 (E) biological replicates.

Figure 2. Treatment with AA, but not ES8, can rescue the IAA level in *wei2wei7*. (A-B) IAA concentrations in 9-day-old seedlings of Col-0 and *wei2wei7* grown on AA (A) or ES8 (B) -supplemented medium. Concentrations are presented as pg per mg fresh weight (FW). Asterisks indicate samples significantly different from the Col-0 mock-treated control unless indicated otherwise (**p<0.01, *p<0.05). Error bars indicate standard error of the mean of the biological replicates. Values in square brackets indicate treatment concentrations in µM. Tissue was sampled from a mixture of 20 ground seedlings per sample per each of 5 (A) or 4 (B) biological replicates.

Figure 3. AA affects gravitropically stimulated root bending independently of IAA biosynthesis. (A-F) Categories of root bending angles for gravistimulated control and 20 µM estradiol-treated seedlings of Col-0 (A-B), *AxP1* (C-D) and *AxP2* (E-F). Polygonal x-axis frequency graphs showing root bending angles in 15° categories (A, C, E) and percentages of roots under-bending at 0-75° angles, bending at approximate right angles of 75-105° and over-bending at 105-360° (B, D, F). Five-day-old seedlings were transferred vertically to mock- (control) or 20 µM estradiol-supplemented medium for 24 h and then gravistimulated by turning 90° clockwise for a further 24 h before measuring gravistimulated root bending angles (see Fig. S6 D). Frequencies/percentages were calculated based on the full dataset of all seedlings measured. *n* = 20 seedlings per sample per each of 3 biological replicates.

Figure 4. AA treatment or deficiency affects basal polarity of PIN auxin transporters in root provascular cells. (A-C) Representative images of immunolabeled PIN1 (A), GFP fluorescence in *PIN3::PIN3-GFP* (B) and immunolabeled PIN7 (C) in stele provascular cells of 5-day-old Col-0 and *wei2wei7* seedling roots. Scale bars represent 10 µm. **(D-F)** Basal polarity index (expressed as a

percentage of the Col-0 mock-treated control) of fluorescence intensities of anti-PIN1 (D), GFP in *PIN3::PIN3-GFP* (E) and anti-PIN7 (F) in stele provascular cells of 5-day-old Col-0 and *wei2wei7* seedling roots treated for 2 h in liquid treatment medium. Asterisks indicate samples significantly different from the Col-0 mock-treated control unless indicated otherwise (***p<0.001, **p<0.01). Error bars indicate standard error of the mean of the biological replicates. Values in square brackets indicate concentrations in µM. *n* = 50 cells per each of 15 seedlings per sample per each of 3 biological replicates.

Figure 5. AA regulates gravistimulated relocalization of PIN auxin transporters in root columella cells. (A-B) Representative images of GFP fluorescence in *PIN3::PIN3-GFP* (A) and *PIN7::PIN7-GFP* (B) in columella cells of 5-day-old Col-0 and *wei2wei7* seedling roots. Scale bars represent 10 µm. **(C-D)** Apical-basal polarity index (expressed as a percentage of the Col-0 mock-treated control) of fluorescence intensities of GFP in *PIN3::PIN3-GFP* (C) and *PIN7::PIN7-GFP* (D) in columella cells of 5-day-old seedlings of Col-0 and *wei2wei7* grown on solid treatment medium. **(E-F)** Fluorescence intensity relocalization (lateral plasma membrane fluorescence after gravistimulation expressed as a percentage of the same plasma membrane fluorescence before gravistimulation) of GFP in *PIN3::PIN3-GFP* (E) and *PIN7::PIN7-GFP* (F) in columella cells of 5-day-old seedlings of Col-0 and *wei2wei7* grown on solid treatment medium and gravistimulated at 90° for 30 min. Lateral refers to the cellular position of the plasma membrane in vertically positioned roots. Asterisks indicate samples significantly different from the Col-0 mock-treated control unless indicated otherwise (***p<0.001, **p<0.01, *p<0.05). Error bars indicate standard error of the mean of the biological replicates. Values in square brackets indicate concentrations in µM. *n* = 5 cells per each of 20 seedlings per sample per each of 3 biological replicates.

Supplemental Figure Legends

Figure S1. AA and other IAA precursors are deficient in *wei2wei7*. Concentrations of anthranilic acid (AA), tryptophan (Trp), tryptamine (Tra), indole-3-acetonitrile (IAN), indole-3-acetamide (IAM) and 2-oxoindole-3-acetic acid (oxIAA) in 9-day-old seedlings of Col-0 and *wei2wei7*. Concentrations are presented as pg per mg fresh

weight (FW). Asterisks indicate significant differences from Col-0 (**p<0.01, *p<0.05). Error bars indicate standard error of the mean of the biological replicates. Tissue was sampled from a mixture of 20 ground seedlings per sample per each of 4 biological replicates.

Figure S2. Effects of AA and ES8 on root gravitropic growth and length in WT seedlings. (A-B) Root gravitropic index and length in 9-day-old seedlings of Col-0 grown on medium supplemented with a range of concentrations of AA (A) or ES8 (B). Asterisks indicate samples significantly different from the mock-treated control (Ctrl) (***p<0.001, **p<0.01, *p<0.05). Error bars indicate standard error of the mean of the biological replicates. Values in square brackets indicate treatment concentrations in µM. *n* = 25 seedlings per sample per each of 3 (A) or 6 (B) biological replicates.

Figure S3. AA but not Trp analogs rescue root gravitropic growth but not length in *wei2wei7*. (A-B) Chemical structures of ES8.7 (A) and ES8.7-Trp (B) and representative images of 9-day-old *wei2wei7* seedlings grown on ES8.7 (A) and ES8.7-Trp (B) -supplemented medium. Scale bar represents 1 cm. **(C-F)** Root gravitropic index and length in 9-day-old seedlings of Col-0 (C, E) and *wei2wei7* (D, F) grown on medium supplemented with a range of concentrations of ES8.7 (C, D) or ES8.7-Trp (E, F). Asterisks indicate samples significantly different from the mock-treated control (Ctrl) (***p<0.001, **p<0.01, *p<0.05). Error bars indicate standard error of the mean of the biological replicates. Values in square brackets indicate concentrations in µM. *n* = 25 seedlings per samples per each of 7 (C, D) or 3 (E, F) biological replicates.

Figure S4. The ES8 compounds are not degraded/metabolized to release AA or Trp. Samples of Col-0 and *wei2wei7* seedlings after short-term (5-day-old seedlings incubated 5 h in liquid treatment medium) or long-term (9-day-old seedlings grown on solid treatment medium) treatments with ES8 compounds were analyzed for the presence of various compounds. Samples of the short-term and long-term treatment medium, which were incubated for the same length of time but without any seedlings added, were also analyzed. **(A)** ES8 analysis in ES8-treated samples. **(B)** ES8.7 analysis in ES8.7-treated samples. **(C)** ES8.7-Trp analysis in ES8.7-Trp-treated samples. **(D)** AA

analysis after mock treatment (control) or treatment with ES8 or ES8.7. AA was not detected (ND) in the treatment medium samples. **(E)** Trp analysis after mock treatment (control) or treatment with ES8.7-Trp. Trp was not detected (ND) in the treatment medium samples. **(F)** Analysis of the non-AA/Trp part of the relevant ES8 compound after treatment with that ES8 compound. The non-AA/Trp parts of the compounds were not detected (ND) in any sample. Concentrations are presented as nmol per g fresh weight (FW) for seedling samples and µM for medium samples. Asterisks indicate long-term-treated samples significantly different from the corresponding short-term-treated samples (A-C) (***p<0.001, **p<0.01, *p<0.05). No significant differences were found between ES8/ES8.7/ES8.7-Trp-treated and the corresponding mock-treated control samples (D-E). Error bars indicate standard error of the mean of the biological replicates. Values in square brackets indicate concentrations in µM. *n* = 100 Col-0 or 250 *wei2wei7* 5-day-old seedlings or 50 Col-0 or 150 *wei2wei7* 9-day-old seedlings per sample per each of 2 biological replicates, with 2 technical replicates analyzed per biological replicate.

Figure S5. Expression levels of *ASA1* and *PAT1* in *AxP* lines. (A) Normalized expression levels of *ASA1* and *PAT1* in 7-day-old *35S::ASA1* seedlings. **(B)** Normalized expression levels of *ASA1* and *PAT1* in 7-day-old non-induced (-) and estradiol-induced (+) *XVE::amiRNA-PAT1* seedlings. **(C-D)** Normalized expression levels of *ASA1* (C) and *PAT1* (D) in 7-day-old non-induced (-) and estradiol-induced (+) *35S::ASA1* x *XVE::amiRNA-PAT1* (*AxP*) seedlings. The lines marked with squares were selected for further analysis (*AxP1*: 3B6x2D4 line no. 4; *AxP2*: 3B7x2D4 line no. 21). For estradiol induction of *PAT1* silencing, seedlings were grown on 20 µM estradiol-supplemented medium. Expression values relative to the Col-0 non-induced control are shown. Asterisks indicate samples significantly different from the Col-0 non-induced control (***p<0.001, **p<0.01, *p<0.05). Error bars indicate standard error of the mean of the biological replicates. *n* = 20 seedlings per sample per each of 3 biological replicates.

Figure S6. IAA metabolite levels and root phenotypes of *AxP* lines. (A) Concentrations of anthranilic acid (AA), tryptophan (Trp), indole-3-acetonitrile (IAN), indole-3-acetamide (IAM), indole-3-acetic acid (IAA), IAA-Aspartate (IAAsp), IAA-

Glutamate (IAGlu) and 2-oxoindole-3-acetic acid (oxIAA) in 5-day-old seedlings of Col-0, *AxP1* and *AxP2* grown on 20 µM estradiol-supplemented medium. IAAsp levels were below the limit of detection (LOD) in the *AxP* lines. Concentrations are presented as pg per mg fresh weight (FW). **(B-C)** Root gravitropic index (B) and length (C) in 9-day-old Col-0, *AxP1* and *AxP2* seedlings grown on mock Asterisks indicate long-term-treated samples significantly different from the corresponding short-term-treated samples (Control) and 20 µM estradiol-supplemented medium. **(D)** Scheme representing root bending angle (α) measurements in Col-0 and *AxP* lines after a 90° gravistimulus (black arrow). Angles were measured at the pre-gravistimulus root tip position (red arrows). Different letters indicate significant differences ($p<0.05$). Error bars indicate standard error of the mean of the biological replicates. Tissue was sampled from a mixture of 20 ground seedlings per sample per each of 3 biological replicates (A). *n* = 20 seedlings per each of 3 biological replicates (B-C).

Figure S7. Expression pattern of the auxin-responsive promoter *DR5* is altered in the root by ES8 treatment or AA deficiency. (A-B) Representative images of GFP fluorescence of *DR5::GFP* in full roots (A) and root tips (B) of 5-day-old Col-0 and *wei2wei7* seedlings grown on mock (Control), ES8 or AA-supplemented medium. Scale bars represent 200 µm (A) and 20µm (B). Tiled compilations of images were used to visualize the full roots (A). Accumulations of GFP signal in cell file initials surrounding the QC are marked by white arrows (B). Values in square brackets indicate concentrations in µM. *n* = 3 (A) or 10 (B) seedlings imaged per sample per each of 4 (A) or 3 (B) biological replicates.

Figure S8. Expression levels of *PIN* genes in Col-0 and *wei2wei7*. (A) Normalized expression levels of *PIN1*, *PIN2*, *PIN3*, *PIN4* and *PIN7* in 9-day-old Col-0 and *wei2wei7* seedlings. **(B)** Normalized expression levels of *PIN1*, *PIN3* and *PIN7* in 5-day-old Col-0 and *wei2wei7* seedlings treated for 2 h in liquid treatment medium. Expression values relative to Col-0 (A) or the Col-0 mock-treated control (B) are shown. Graphs show mean of 4 biological replicates and standard error of the mean. Asterisks indicate significantly different from Col-0 (**$p<0.01$, *$p<0.05$). Error bars indicate standard error of the mean of the biological replicates. Values in square

brackets indicate concentrations in µM. *n* = 30 seedlings per sample per each of 4 biological replicates.

Figure S9. Expression patterns of *ASA1* and *ASB1* in the root and immunolocalization of PIN3, PIN4 and PIN7 in the columella. (A-C) Representative images of GUS-stained upper roots (A), lower roots (B) and root tips (C) of 9-day-old *ASA1::GUS* and *ASB1::GUS* seedlings. Scale bars represent 30 µm. **(D-F)** Representative images (merged transmission light and Cy3 channel images) of immunolabeled PIN3 (D), PIN4 (E) and PIN7 (F) in root tips of 5-day-old Col-0 or *wei2wei7* seedlings. Scale bars represent 10 µm. *n* = 10 seedlings imaged per sample per each of 3 biological replicates.

Figure S10. Root gravitropic growth in *pin* and *wei2wei7pin* mutants. (A) Root gravitropic index in 5-day-old seedlings of *pin* mutants and *pin* mutants crossed into *wei2wei7*. **(B-C)** Root gravitropic index (expressed as a percentage of that in mock-treated samples of the same line) in 5-day-old seedlings of *pin* and *wei2wei7pin* mutants grown on 15 µM ES8 (B) and 20 µM AA (C) -supplemented medium. Asterisks and hash symbols indicate significant differences from Col-0 (***$p<0.001$, **$p<0.01$, *$p<0.05$) or *wei2wei7* ($^{###}p<0.001$, $^{##}p<0.01$, $^{#}p<0.05$), respectively. Error bars indicate standard error of the mean of the biological replicates. *n* = 30 seedlings per sample per each of 3 biological replicates.

Supplemental Tables

Table S1. *Arabidopsis* mutants and transformed lines used in this study.

Table S2. Genotyping, cloning and qPCR primers used in this study.

FIGURE 1

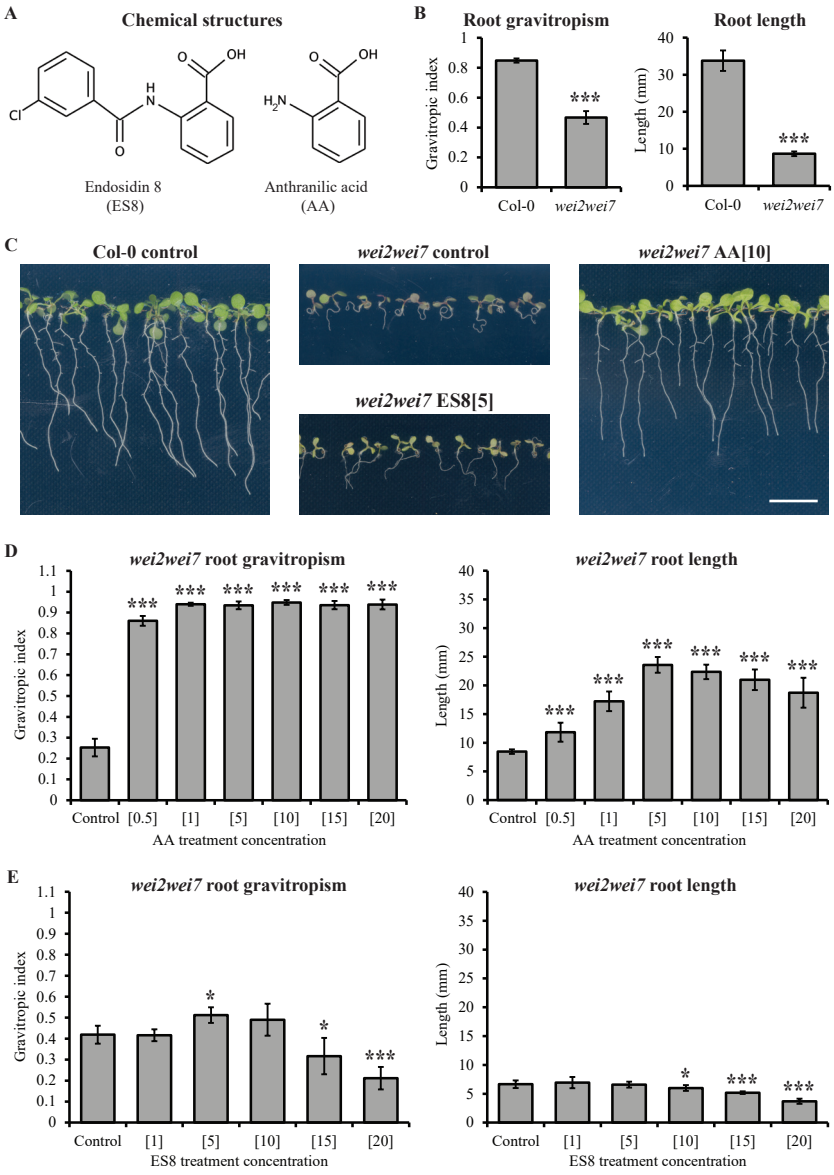

FIGURE 2

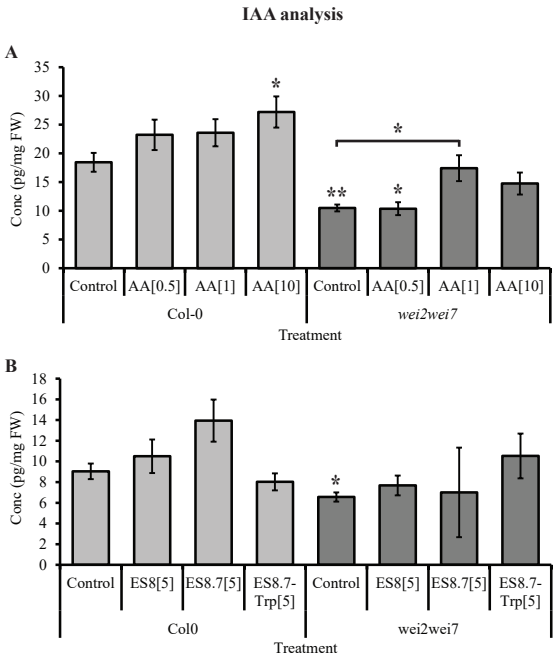

FIGURE 3

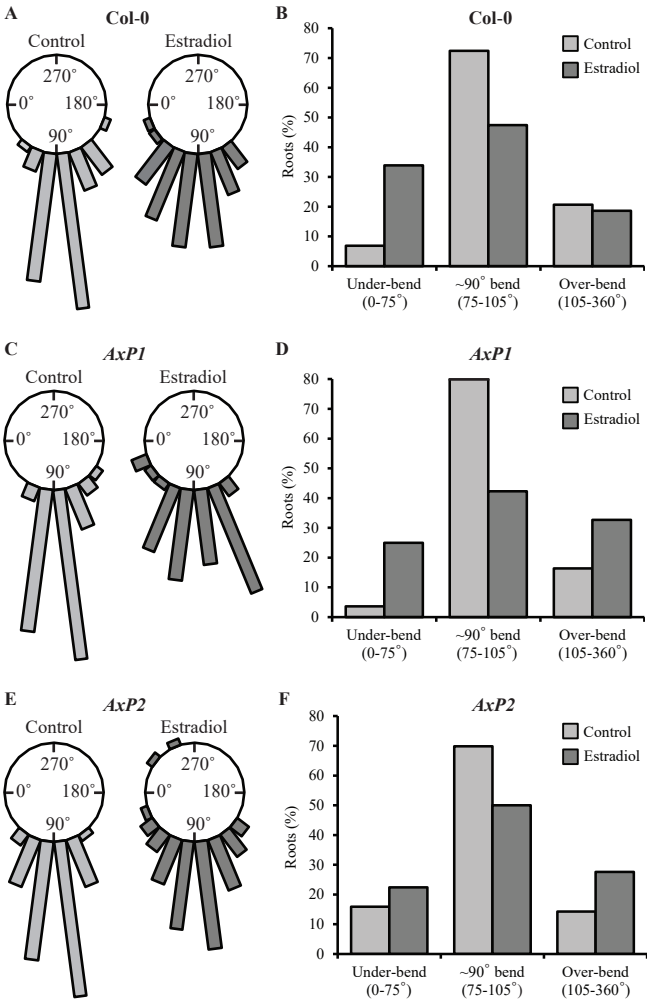

FIGURE 4

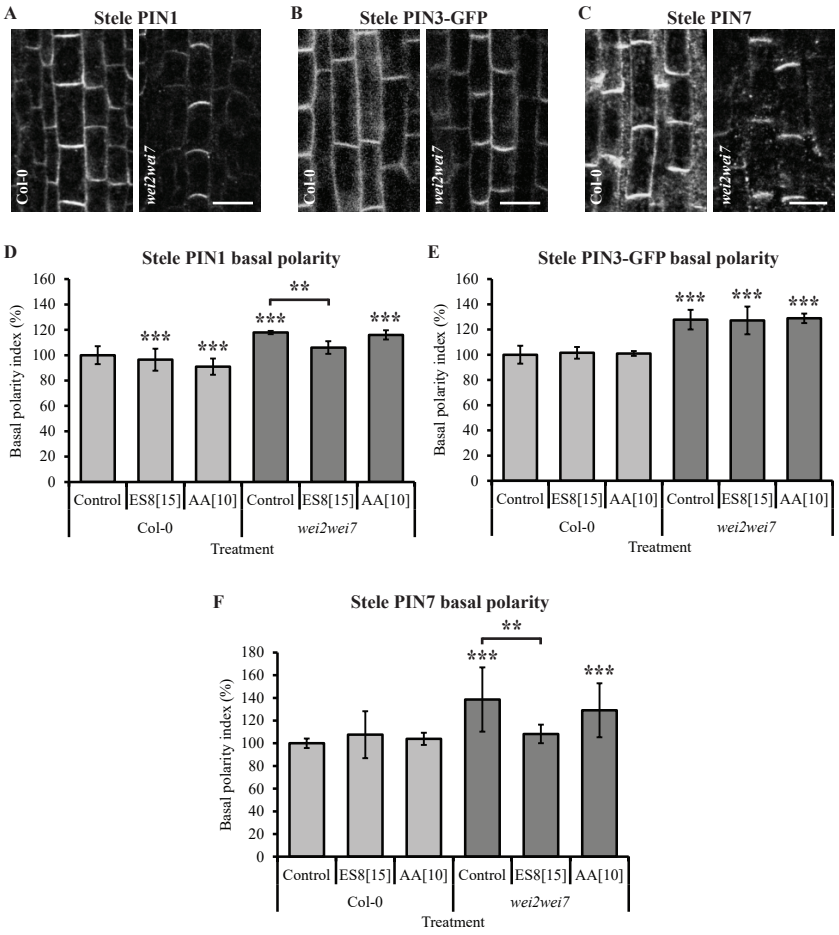

FIGURE 5

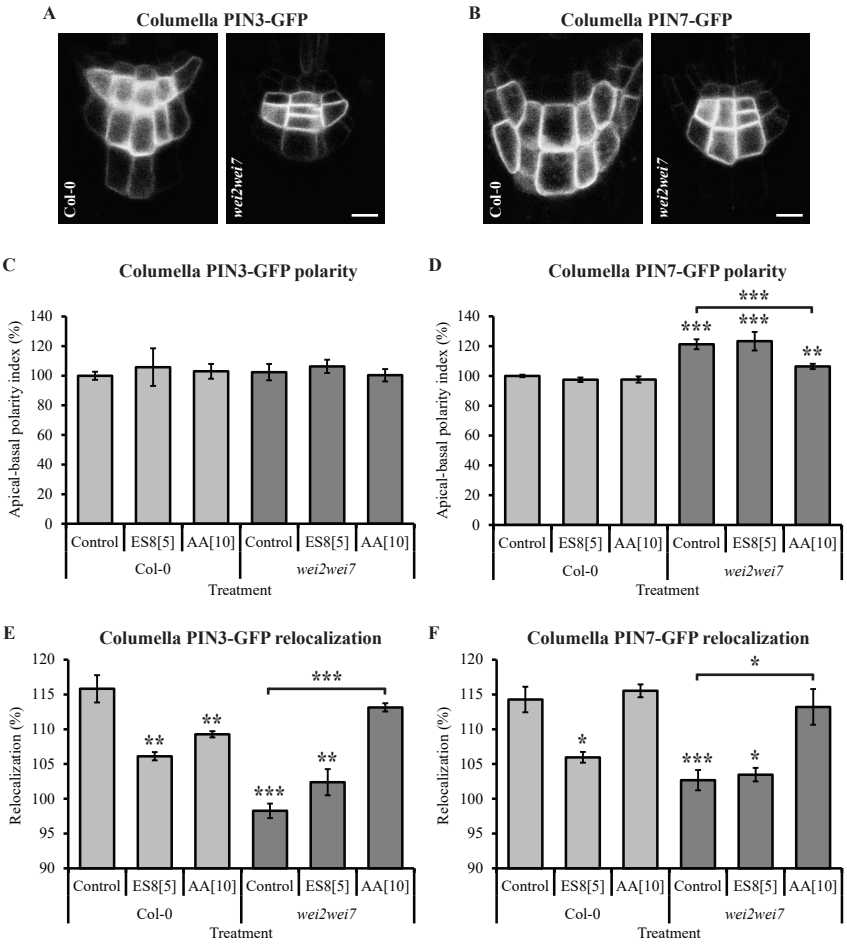

FIGURE S1

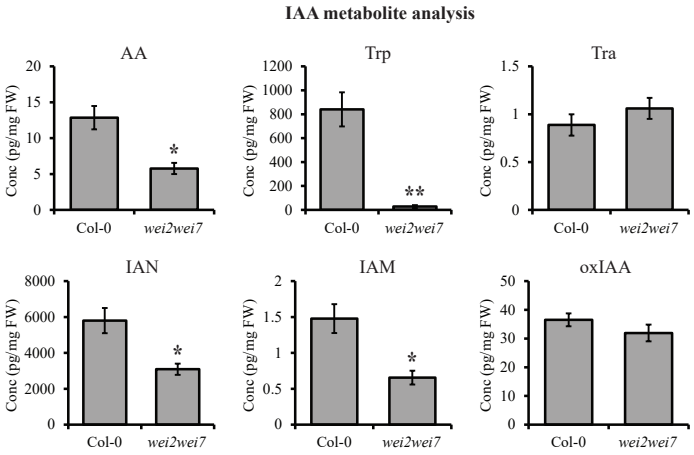

FIGURE S2

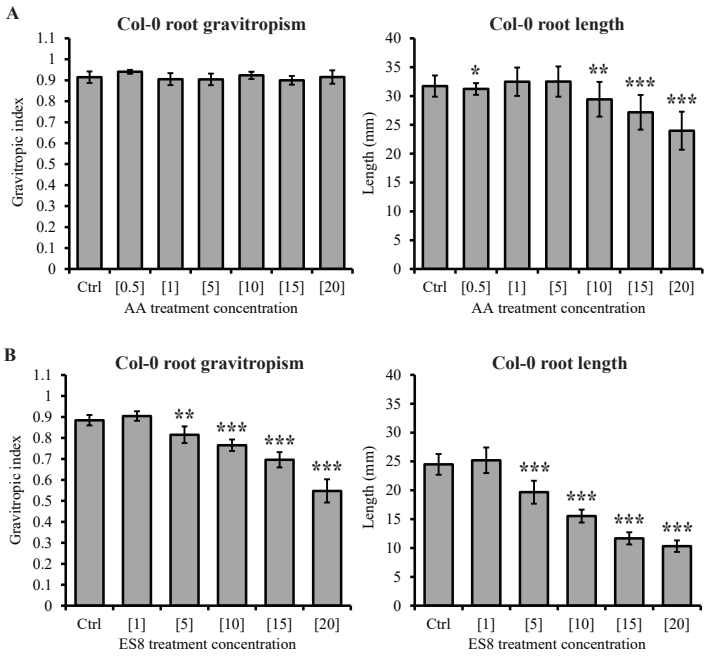

FIGURE S3

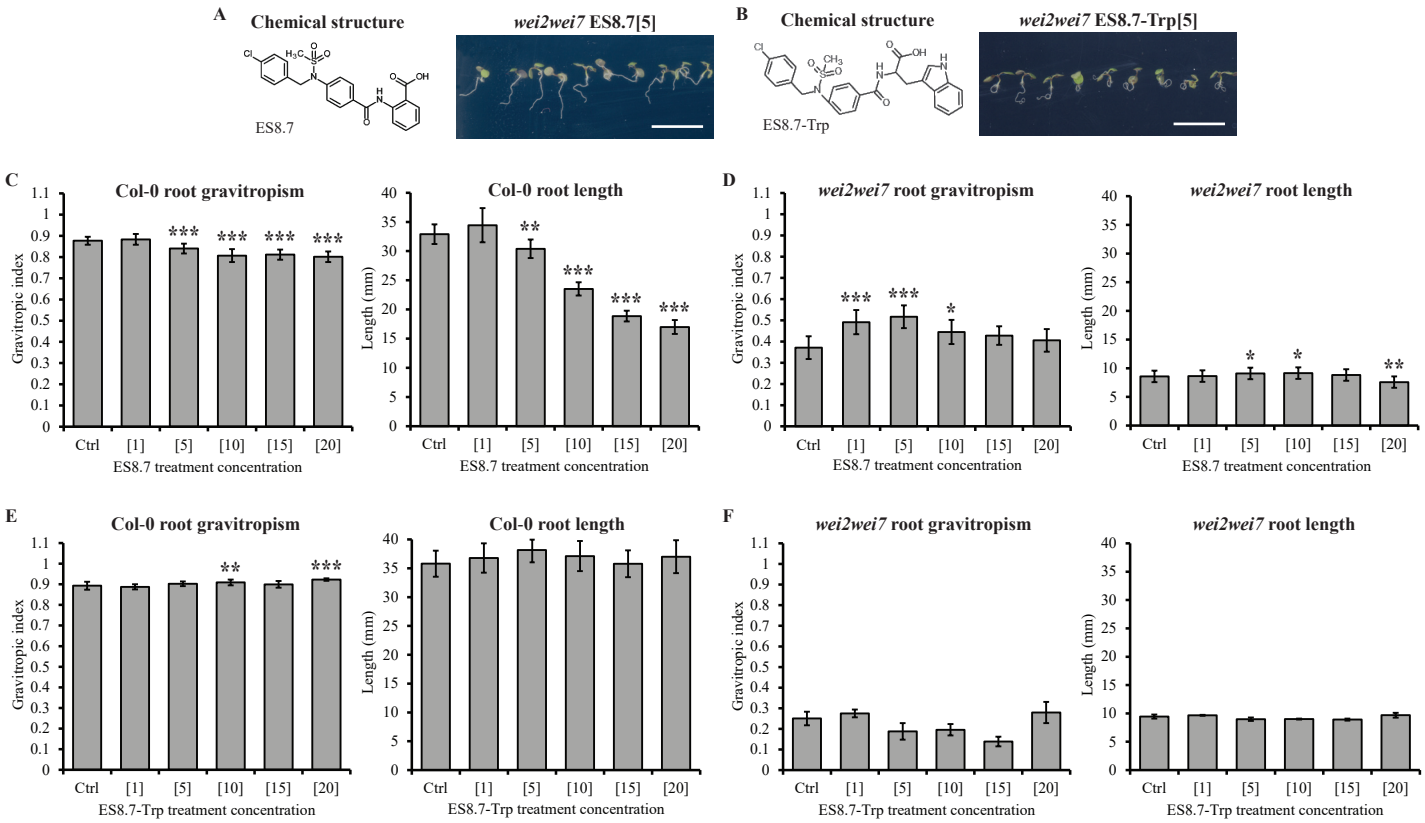

FIGURE S4

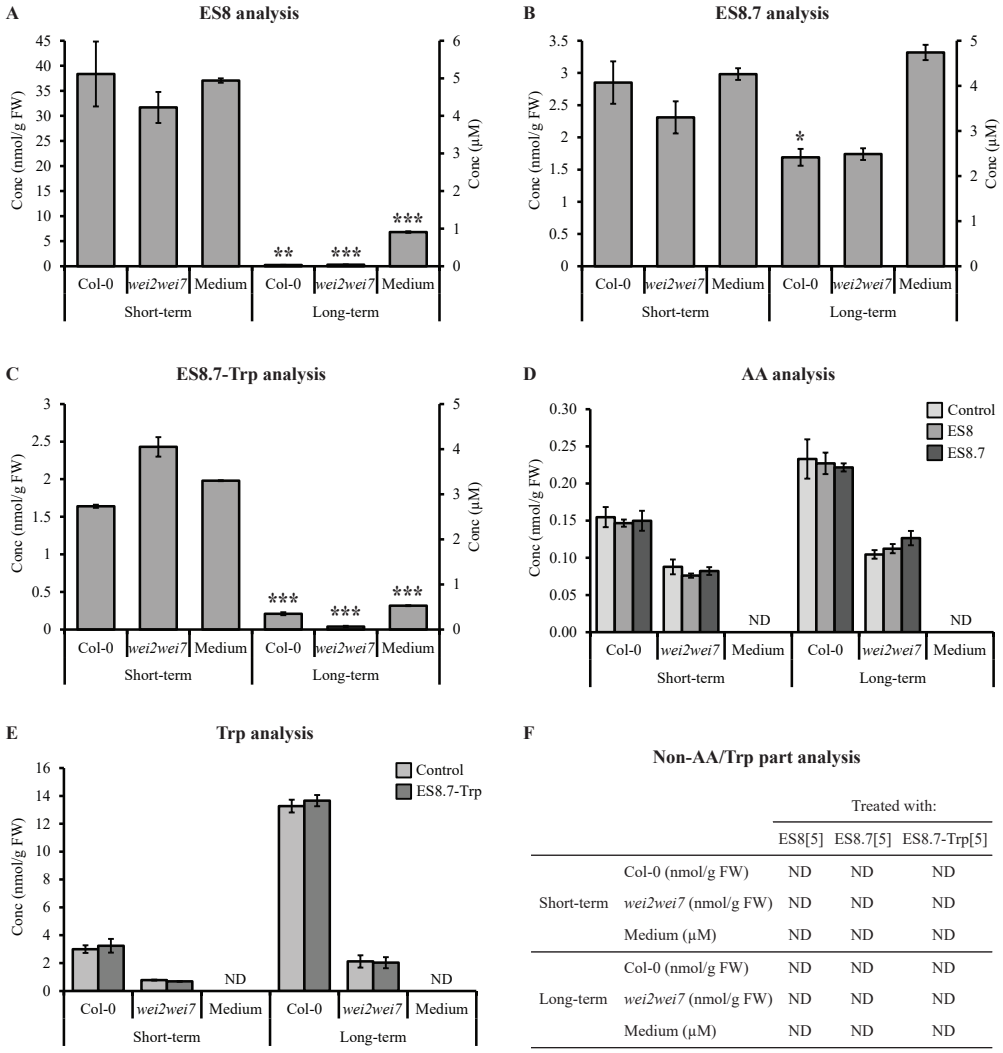

		Treated with:		
		ES8[5]	ES8.7[5]	ES8.7-Trp[5]
Short-term	Col-0 (nmol/g FW)	ND	ND	ND
	wei2wei7 (nmol/g FW)	ND	ND	ND
	Medium (μM)	ND	ND	ND
Long-term	Col-0 (nmol/g FW)	ND	ND	ND
	wei2wei7 (nmol/g FW)	ND	ND	ND
	Medium (μM)	ND	ND	ND

FIGURE S5

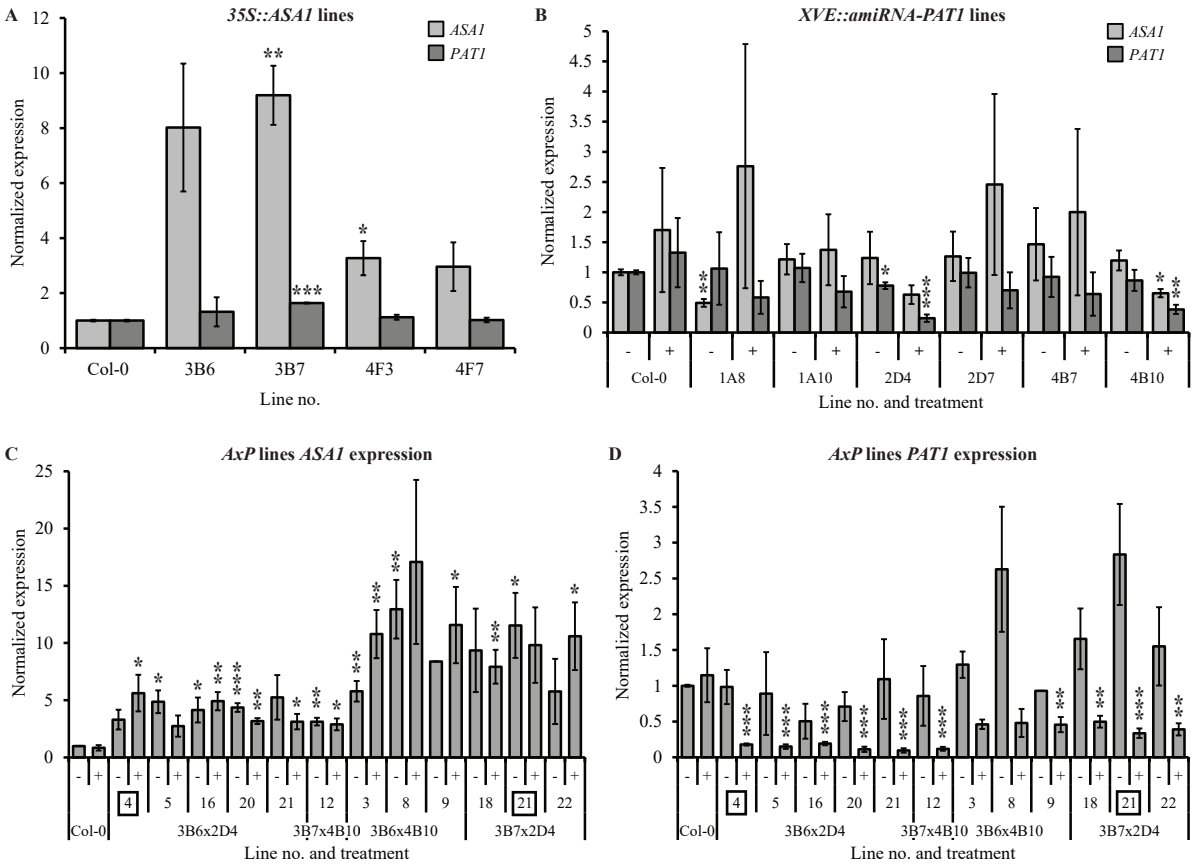

FIGURE S6

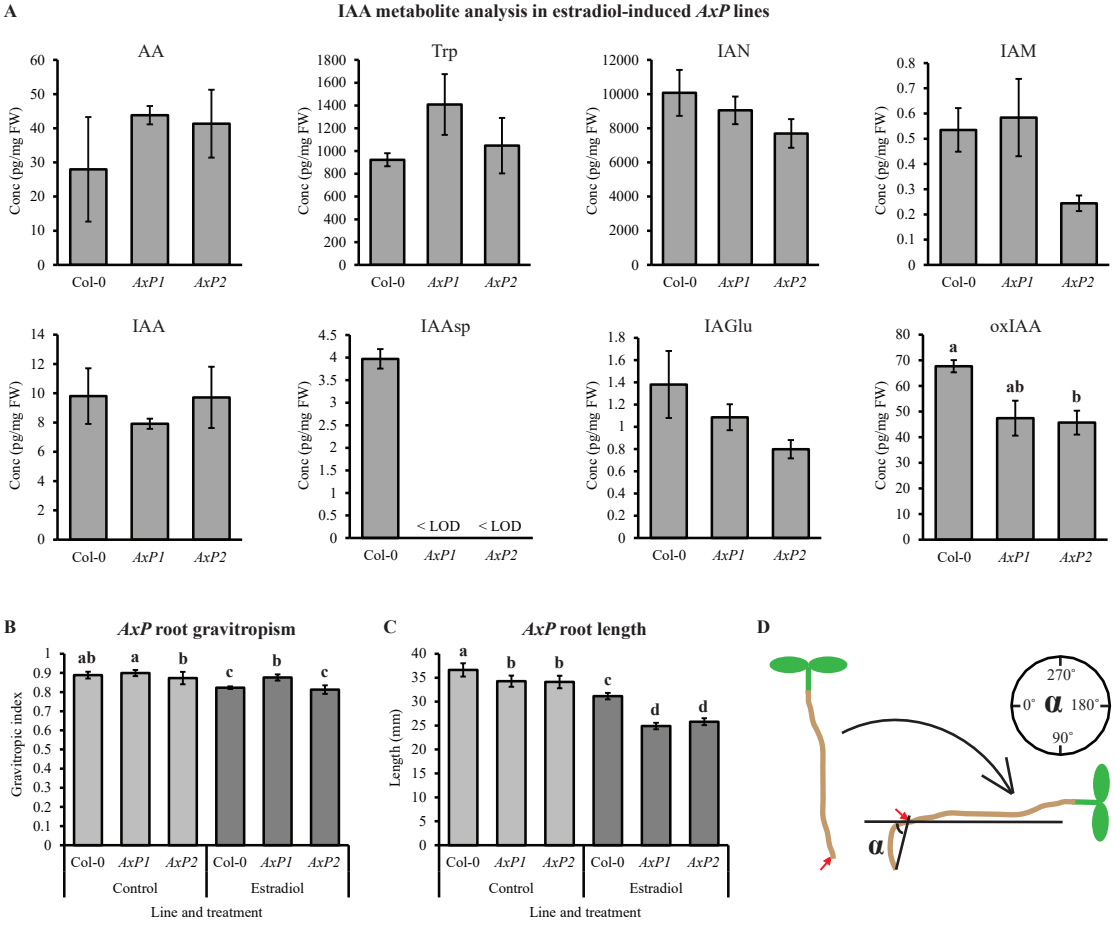

FIGURE S7

A **Root *DR5::GFP* auxin response pattern**

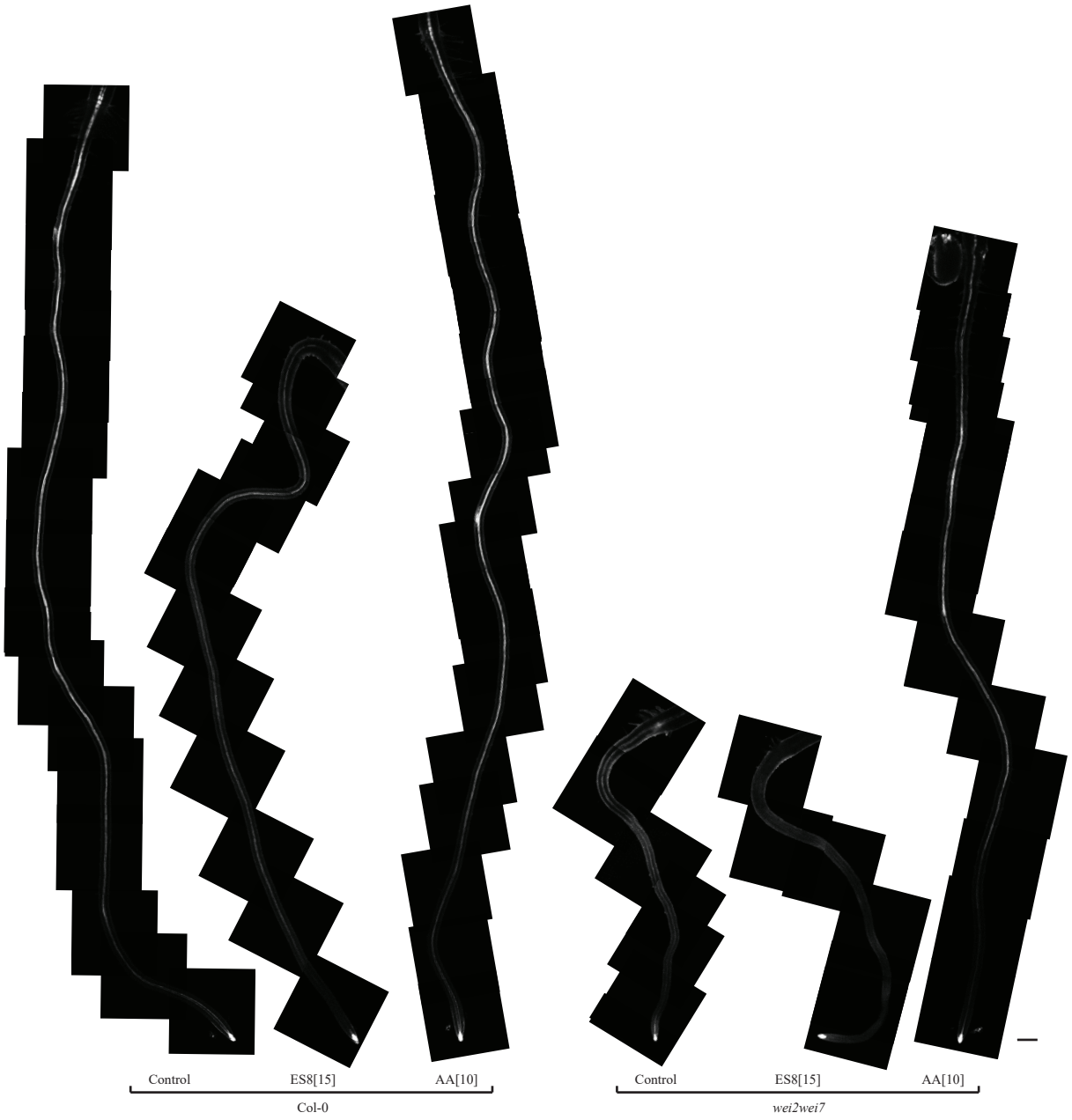

B **Root tip *DR5::GFP* auxin response pattern**

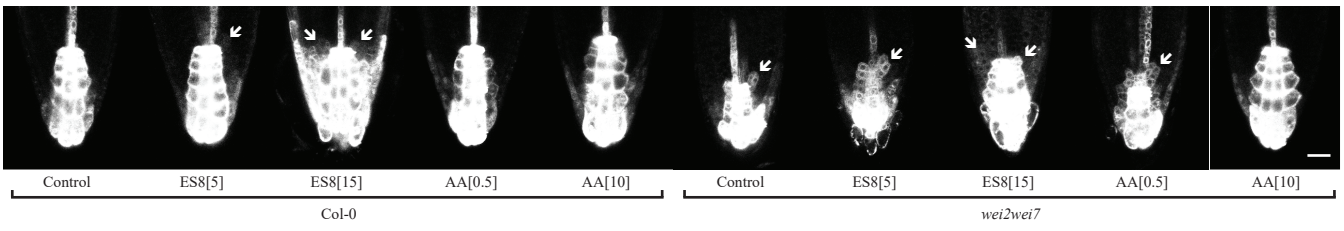

FIGURE S8

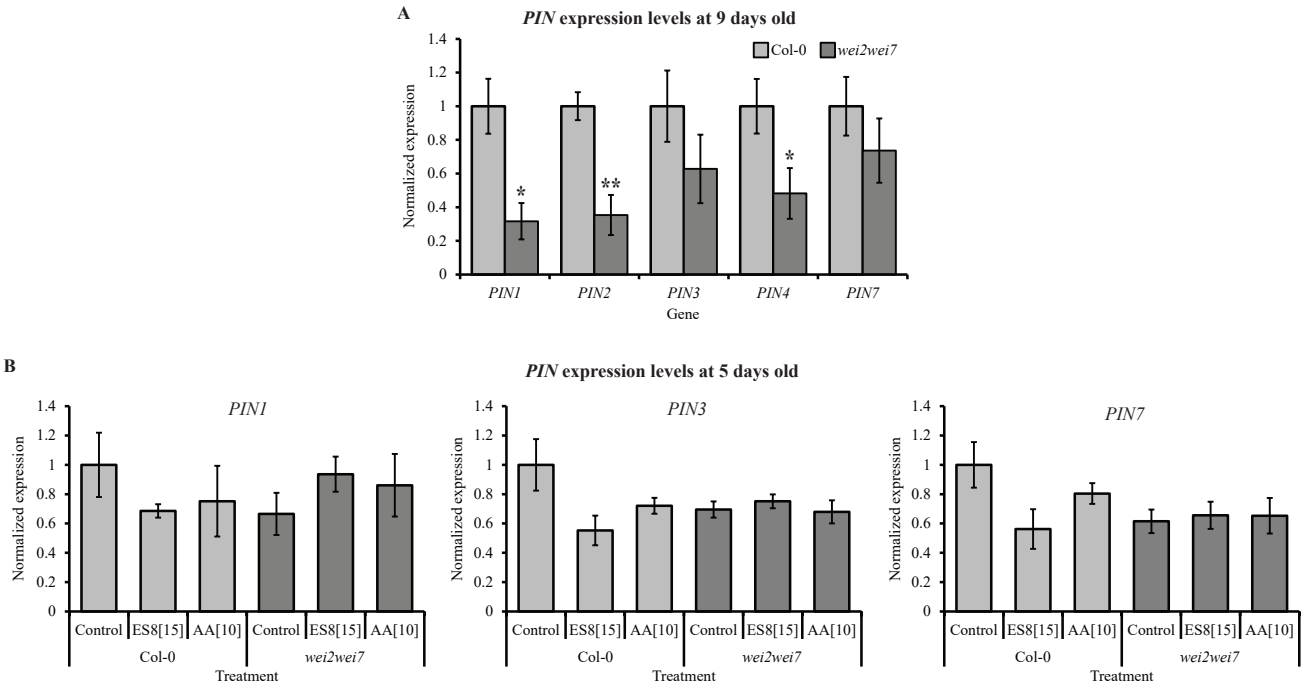

FIGURE S9

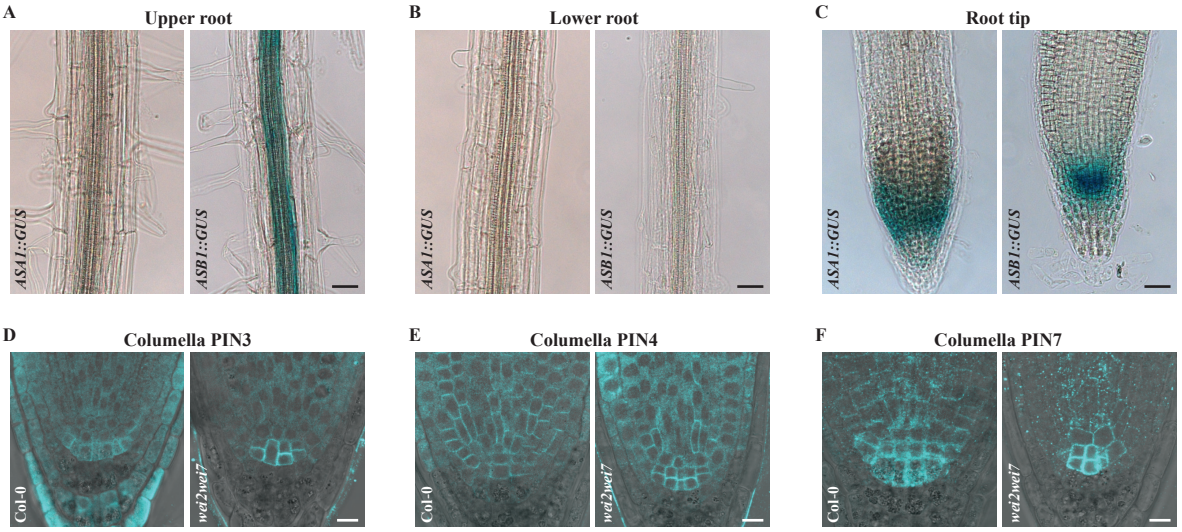

FIGURE S10

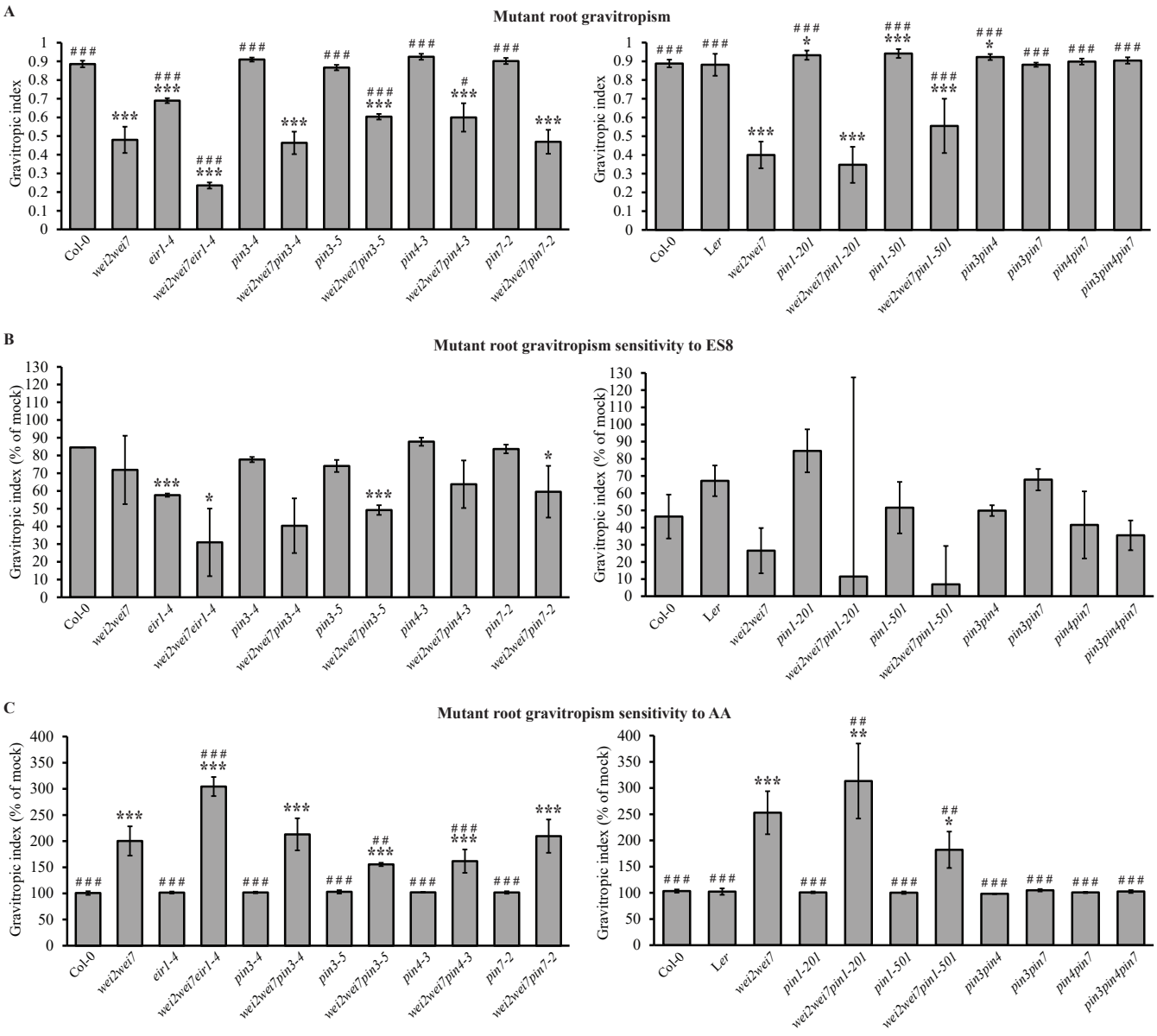

Table S1. *Arabidopsis* mutants (A) and transformed lines (B) used in this study. SALK/SAIL T-DNA insertion lines (Alonso et al., 2003) were obtained from NASC. Arabidopsis Genome Initiative (AGI) codes are included for all genes. We renamed *pin1-5* SALK line 097144 to *pin1-501* to distinguish the mutant from another published *pin1-5* allele. *These crosses were kindly provided by Jiří Friml.

A) Mutants

Mutant name	ID / mutation type	Gene name(s)	AGI code(s)	Reference(s)
wei2-1wei7-1	point mutation, deletion	*ASA1*, *ASB1*	AT5G05730, AT1G25220	Stepanova et al. (2005)
pin1-201	SALK_047613/047843	*PIN1*	AT1G73590	Furutani et al. (2004)
pin1-501	SALK_097144	*PIN1*	AT1G73590	Xu et al. (2010), Zourelidou et al. (2009)
eir1-4	SALK_091142/547613	*PIN2*	AT5G57090	Abas et al. (2006)
pin3-4	SALK_038609	*PIN3*	AT1G70940	Friml et al. (2003)
pin3-5	SALK_005544	*PIN3*	AT1G70940	Friml et al. (2003)
pin4-3	En-1 transposon insertion	*PIN4*	AT2G01420	Friml et al. (2002)
pin3-5pin4-3	see above	see above	see above	Le et al. (2014)
pin7-2	SALK_044687	*PIN7*	AT1G23080	Friml et al. (2003)
*pin3-5pin7-2**	see above	see above	see above	----
*pin4-3pin7-2**	see above	see above	see above	----
pin3-5pin4-3pin7-1	(*pin7-1*: transposable Ds element insertion)	(*pin7-1*: *PIN7*)	(*pin7-1*: AT1G23080)	Friml et al. (2003)

B) Transformed lines

Line name	AGI code	Reference
DR5rev::GFP	----	Friml et al. (2003)
PIN3::PIN3-GFP	*PIN3*: AT1G70940	Žádníková et al. (2010)
PIN7::PIN7-GFP	*PIN7*: AT1G23080	Blilou et al. (2005)
ASA1::GUS	*ASA1*: AT5G05730	Stepanova et al. (2005)
ASB1::GUS	*ASB1*: AT1G25220	Stepanova et al. (2005)

Table S1 References

Abas, L., R. Benjamins, N. Malenica, T. Paciorek, J. Wiśniewska, J. C. Moulinier-Anzola, T. Sieberer, J. Friml, and C. Luschnig. 2006. Intracellular trafficking and proteolysis of the *Arabidopsis* auxin-efflux facilitator PIN2 are involved in root gravitropism. *Nat Cell Biol,* 8**,** 249-56.

Alonso, J. M., A. N. Stepanova, T. J. Leisse, C. J. Kim, H. Chen, P. Shinn, D. K. Stevenson, J. Zimmerman, P. Barajas, R. Cheuk, C. Gadrinab, C. Heller, A. Jeske, E. Koesema, C. C. Meyers, H. Parker, L. Prednis, Y. Ansari, N. Choy, H. Deen, M. Geralt, N. Hazari, E. Hom, M. Karnes, C. Mulholland, R. Ndubaku, I. Schmidt, P. Guzman, L. Aguilar-Henonin, M. Schmid, D. Weigel, D. E. Carter, T. Marchand, E. Risseeuw, D. Brogden, A. Zeko, W. L. Crosby, C. C. Berry, and J. R. Ecker. 2003. Genome-Wide Insertional Mutagenesis of Arabidopsis thaliana. *Science,* 301**,** 653-657.

Blilou, I., J. Xu, M. Wildwater, V. Willemsen, I. Paponov, J. Friml, R. Heidstra, M. Aida, K. Palme, and B. Scheres. 2005. The PIN auxin efflux facilitator network controls growth and patterning in *Arabidopsis* roots. *Nature,* 433**,** 39-44.

Friml, J., E. Benková, I. Blilou, J. Wisniewska, T. Hamann, K. Ljung, S. Woody, G. Sandberg, B. Scheres, G. Jürgens, and K. Palme. 2002. AtPIN4 mediates sink-driven auxin gradients and root patterning in *Arabidopsis*. *Cell,* 108**,** 661-673.

Friml, J., A. Vieten, M. Sauer, D. Weijers, H. Schwarz, T. Hamann, R. Offringa, and G. Jürgens. 2003. Efflux-dependent auxin gradients establish the apical-basal axis of *Arabidopsis*. *Nature,* 426**,** 147-53.

Furutani, M., T. Vernoux, J. Traas, T. Kato, M. Tasaka, and M. Aida. 2004. PIN-FORMED1 and PINOID regulate boundary formation and cotyledon development in Arabidopsis embryogenesis. *Development,* 131**,** 5021-30.

Le, J., X. G. Liu, K. Z. Yang, X. L. Chen, J. J. Zou, H. Z. Wang, M. Wang, S. Vanneste, M. Morita, M. Tasaka, Z. J. Ding, J. Friml, T. Beeckman, and F. Sack. 2014. Auxin transport and activity regulate stomatal patterning and development. *Nat Commun,* 5**,** 3090.

Stepanova, A. N., J. M. Hoyt, A. A. Hamilton, and J. M. Alonso. 2005. A Link between ethylene and auxin uncovered by the characterization of two root-specific ethylene-insensitive mutants in Arabidopsis. *Plant Cell,* 17**,** 2230-42.

Xu, T., M. Wen, S. Nagawa, Y. Fu, J.-G. Chen, M.-J. Wu, C. Perrot-Rechenmann, J. Friml, A. M. Jones, and Z. Yang. 2010. Cell surface- and rho GTPase-based auxin signaling controls cellular interdigitation in *Arabidopsis*. *Cell,* 143**,** 99-110.

Žádníková, P., J. Petrášek, P. Marhavý, V. Raz, F. Vandenbussche, Z. Ding, K. Schwarzerová, M. T. Morita, M. Tasaka, J. Hejátko, D. Van Der Straeten, J. Friml, and E. Benková. 2010. Role of PIN-mediated auxin efflux in apical hook development of *Arabidopsis thaliana*. *Development,* 137**,** 607-617.

Zourelidou, M., I. Müller, B. C. Willige, C. Nill, Y. Jikumaru, H. Li, and C. Schwechheimer. 2009. The polarly localized D6 PROTEIN KINASE is required for efficient auxin transport in *Arabidopsis thaliana*. *Development,* 136**,** 627-36.

Table S2. Genotyping (A), cloning (B) and qPCR (C) primers used in this study. Primers marked SALK or CSH were sourced from the SALK Institute Genomic Analysis Laboratory website (http://signal.salk.edu/) or the Cold Spring Harbor Arabidopsis Genetrap website (http://genetrap.cshl.org/), respectively. Primers with no indicated source have not been published previously (sequences designed in the present study or kindly provided by collaborators). Arabidopsis Genome Initiative (AGI) codes are included (for affected gene AGIs in mutants listed in (A) see Supplemental Tale S1).

A) Genotyping primers

Mutation	Reactions/Digestion	Forward	Reverse	Source
wei2-1	F+R, digest with XbaI	GTGAATCCAAGTCCGTATATGGGTTATTTCTAG	TGCATCCTCTAGCCTGAATAACAG	Ikeda et al. (2009)
wei7-1	F+R1, F+R2	CTCTCCTCTTACCCATCCTTGAGGTTC	GCATGTCGAAACTAGATTGGATTGTG GCATGACTTCATGTATTCTGAGTTTGCC	Ikeda et al. (2009)
pin1-201	F+R, LBb1.3+R	CAAAAACACCCCCAAAATTTC	AATCATCACAGCCACTGATCC	SALK
pin1-5	F+R, LBb1.3+R	AACTGGCTTCACAGCAGAAAG	AGTTATGGGCAACGCGATCA	SALK
eir1-4	F+R, LBa1+R	CCACCGACCCTAAAGTTTCT	GCAAGGCCAAAGAGACTAGA	----
pin3-4	F+R, LBb1.3+R	TGCCACCTTCAATTCAAAAAC	TGATTTTCTTGAGACCGATGC	SALK
pin3-5	F+R, LBb1.3+R	CCCATCCCCAAAAGTAGAGTG	ATGATACACTGGAGGACGACG	SALK
pin4-3	F+R, En8130+R	AACCGGTACGGGTGTTTCAACTA	GCCATTCCAAGACCAGCATCT	----
pin7-2	F+R, LBb1.3+R	CTCTTTTGCAAACACAAACGG	GGTAAAGGAAGTGCCTAACGG	SALK
pin7-1	F+R, F+Ds5	AAATCCGATCAAGGCGGTG	CGTCGAATTTCCGCAAGC	----

LBa1	TGGTTCACGTAGTGGGCCATCG	SALK
LBb1.3	ATTTTGCCGATTTCGGAAC	SALK
En8130	GAGCGTCGGTCCCCACACTTCTATAC	Baumann et al. (1998)
Ds5	ACGGTCGGGAAACTAGCTCTA	CSH

B) Cloning primers

Gene	AGI code	Forward	Reverse	Remark
ASA1	AT5G05730	CACCATGTCTTCCTCTATGAACGTAGCGA	TCATTTTTTCACAAATGCAGATTCA	coding region
PAT1	AT5G17990	TCTAATAAAGCAAAGCGGCTT		amiRNA sequence
		GATCTAATAAAGCAAAGCGGCTTTCTCTCTTTTGTATTCC	GAAAGCCGCTTTGCTTTATTAGATCAAAGAGAATCAATGA	microRNA I, II
		GAAAACCGCTTTGCTATATTAGTTCACAGGTCGTGATATG	GAACTAATATAGCAAAGCGGTTTTCTACATATATATTCCT	microRNA* III, IV
		CACCCTGCAAGGCGATTAAGTTGGGTAAC	GCGGATAACAATTTCACACAGGAAACAG	oligo A, B
PIN7	AT1G23080	GAGACTGGTGCTTCGATTGTA	CCGAGTCATCACACTCGCTGG	hydrophobic loop
		GGGGACAAGTTTGTACAAAAAAGCAGGCTCCACCAGGAGGATGGAGACTGGTGCTTCGATTGTA		attB1 (forward)
		GGGGACCACTTTGTACAAGAAAGCTGGGTATTACCGAGTCATCACACTCGCTGG		attB2 (reverse)

C) qPCR primers

Gene	AGI code	Forward	Reverse	Reference
PEX4	AT5G25760	CTTAACTGCGACTCAGGGAATCTTC	AGGCGTGTATACATTTGTGCCATT	Doyle et al. (2015)
GADPH	AT1G13440	TTGGTGACAACAGGTCAAGCA	AAACTTGTCGCTCAATGCAATC	Doyle et al. (2015)
TIP41-LIKE	AT4G34270	GGTTCCTCCTCTTGCGATT	ACAGTTGGTGCCTCATCTTC	Doyle et al. (2015)
PP2A PDF2	AT1G13320	TAACGTGGCCAAAATGATGC	GTTCTCCACAACCGCTTGGT	Doyle et al. (2015)
PIN1	AT1G73590	TACTCCGAGACCTTCCAACTACG	TCCACCGCCACCACTTCC	Růžička et al. (2009)
PIN2	AT5G57090	CCTCGCCGCACTCTTTCTTTGG	CCGTACATCGCCCTAAGCAATGG	Růžička et al. (2009)
PIN3	AT1G70940	CCCAGATCAATCTCACAACG	CCGGCGAAACTAAATTGTTG	Lucas et al. (2011)
PIN4	AT2G01420	TTGTCTCTGATCAACCTCGAAA	ATCAAGACCGCCGATATCAT	Lucas et al. (2011)
PIN7	AT1G23080	CGGCTGATATTGATAATGGTGTGG	GCAATGCAGCTTGAACAATGG	Růžička et al. (2009)
ASA1	AT5G05730	ATGCATATAAGCTCCACGGTGAC	GTACGTCCCAGCAAGTCAAACC	present study
PAT1 (1)	AT5G17990	TCAATCTTCCTTTAGTCGCAGCTC	TCCACCGCTCAAACCGAGATTC	present study
PAT1 (2)	AT5G17990	TGGTTTAAGGCGCTTTGCTT	GCCACCGCAATAACCATCAC	present study

Table S2 references

Baumann, E., J. Lewald, H. Saedler, B. Schulz, and E. Wisman. 1998. Successful PCR-based reverse genetic screens using an *En-1*-mutagenised *Arabidopsis thaliana* population generated via single-seed descent. *Theoretical and Applied Genetics,* 97**,** 729-734.

Doyle, S. M., A. Haeger, T. Vain, A. Rigal, C. Viotti, M. Łangowska, Q. Ma, J. Friml, N. V. Raikhel, G. R. Hicks, and S. Robert. 2015. An Early Secretory Pathway Mediated by GNOM-LIKE 1 and GNOM is Essential for Basal Polarity Establishment in *Arabidopsis thaliana*. *Proc Natl Acad Sci U S A,* 112**,** E806-E815.

Ikeda, Y., S. Men, U. Fischer, A. N. Stepanova, J. M. Alonso, K. Ljung, and M. Grebe. 2009. Local auxin biosynthesis modulates gradient-directed planar polarity in *Arabidopsis*. *Nat Cell Biol,* 11**,** 731-8.

Lucas, M., R. Swarup, I. A. Paponov, K. Swarup, I. Casimiro, D. Lake, B. Peret, S. Zappala, S. Mairhofer, M. Whitworth, J. Wang, K. Ljung, A. Marchant, G. Sandberg, M. J. Holdsworth, K. Palme, T. Pridmore, S. Mooney, and M. J. Bennett. 2011. SHORT-ROOT regulates primary, lateral, and adventitious root development in Arabidopsis. *Plant Physiology,* 155**,** 384-98.

Růžička, K., M. Šimášková, J. Duclercq, J. Petrášek, E. Zažímalová, S. Simon, J. Friml, M. C. Van Montagu, and E. Benková. 2009. Cytokinin regulates root meristem activity via modulation of the polar auxin transport. *Proc Natl Acad Sci USA,* 106**,** 4284-9.